nature metabolism

Article

https://doi.org/10.1038/s42255-023-00761-7

NAD$^+$ precursor supplementation prevents mtRNA/RIG-I-dependent inflammation during kidney injury

Received: 10 July 2022

Accepted: 9 February 2023

Published online: 13 March 2023

Check for updates

Tomohito Doke[1,2], Sarmistha Mukherjee[2,3], Dhanunjay Mukhi[1,2], Poonam Dhillon[1,2], Amin Abedini[1,2], James G. Davis[2,3], Karthikeyani Chellappa[2,3], Beishan Chen[2,3], Joseph A. Baur[2,3] ✉ & Katalin Susztak[1,2] ✉

Our understanding of how global changes in cellular metabolism contribute to human kidney disease remains incompletely understood. Here we show that nicotinamide adenine dinucleotide (NAD$^+$) deficiency drives mitochondrial dysfunction causing inflammation and kidney disease development. Using unbiased global metabolomics in healthy and diseased human kidneys, we identify NAD$^+$ deficiency as a disease signature. Furthermore using models of cisplatin- or ischaemia-reperfusion induced kidney injury in male mice we observed NAD$^+$ depletion Supplemental nicotinamide riboside or nicotinamide mononucleotide restores NAD$^+$ levels and improved kidney function. We find that cisplatin exposure causes cytosolic leakage of mitochondrial RNA (mtRNA) and activation of the cytosolic pattern recognition receptor retinoic acid-inducible gene I (RIG-I), both of which can be ameliorated by restoring NAD$^+$. Male mice with RIG-I knock-out (KO) are protected from cisplatin-induced kidney disease. In summary, we demonstrate that the cytosolic release of mtRNA and RIG-I activation is an NAD$^+$-sensitive mechanism contributing to kidney disease.

Genome- and transcriptome-wide association studies have revealed that there is an enrichment of genes causing kidney disease (KD) in proximal tubule cells[1–3]. Tubule cells play a critical role by reabsorbing essential substrates filtered from the blood and excreting waste and toxins into urine. This process is energetically demanding requiring high mitochondrial density[4]. Consequently, kidney tubule cells are vulnerable to injuries cause by hypoxia- or toxin. Moreover, genes linked to KD risk are enriched for metabolic processes such as fatty acid oxidation and oxidative phosphorylation, suggesting that dysregulated renal tubule metabolism plays a causal role in the development of KD.

Dysregulated NAD$^+$ homeostasis has been observed both in humans[5] and various animal KD models[6,7]. In mice several studies have demonstrated a protective role for NAD$^+$ precursor supplementation. Nicotinamide (NAM), nicotinamide riboside (NR) and nicotinamide mononucleotide (NMN) have been shown to protect rodents against kidney injuries[8–13]. While the effects of NAD$^+$ precursor supplementation on human KD are less are less well understood recent data are promising. Kidney injury was reduced by NAMsupplementation in patients undergoing heart surgery[14] and COVID-19-related acute kidney injury (AKI)[15]. Furthermore, NR treatment increased blood NAD$^+$ levels in hospitalized patients with AKI[16]. Although multiple NAD$^+$ precursors showed a protective effect on KD, differences in bioavailability or effectiveness are not well understood. NMN and NR exhibit tissue- or cell-dependent pharmacokinetics and metabolic fates[17], but they have rarely been compared directly and not at all in the context of kidney injury. Moreover, the downstream consequences of changing NAD$^+$ availability are still not well understood. Although various mechanisms by which NAD$^+$ supplementation might protect the kidney in rodent

[1]Department of Medicine, Renal Electrolyte and Hypertension Division, University of Pennsylvania, Philadelphia, PA, USA. [2]Institute for Diabetes, Obesity and Metabolism, University of Pennsylvania, Philadelphia, PA, USA. [3]Department of Physiology, Perelman School of Medicine, University of Pennsylvania, Philadelphia, PA, USA. ✉e-mail: baur@pennmedicine.upenn.edu; ksusztak@pennmedicine.upenn.edu

models have been proposed[8,18] a comprehensive, unbiased analysis of NAD^+ metabolism in human KD is currently lacking.

Mitochondrial dysfunction plays a multifaceted role in the development of KD. At late disease stages, the lack of cellular ATP can lead to cellular dedifferentiation and cell death. Single-cell gene expression analysis highlighted that even at early disease stages some proximal tubules exhibit an injured pro-inflammatory phenotype and may be the origin for fibroinflammation[19]. It was recently discovered that the cytosolic leakage of mtRNA through the apoptosis regulator (BAX) pore can activate the retinoic acid-inducible gene I (RIG-I)-like receptors (RLRs)-mitochondrial antiviral-signalling protein (MAVS) cytosolic RNA-sensing pathway[20,21]. mtRNA binds to RIG-I (encoded by *DDX58*)[20], or melanoma differentiation-associated protein 5 (MDA5, encoded by *IFIH1*)[21]. Some observations suggest that mtRNA may play a more important role in inducing inflammation than does mitochondrial DNA[20]. However, the role of mtRNA in renal tubule cells remains unexplored.

To address these questions, we performed unbiased metabolomic studies using a mouse KD model and kidneys of patients with KD. Our findings revealed consistent changes in NAD^+ metabolism. We also conducted mechanistic experiments to understand how NAD^+ metabolism interacts with mitochondria dysfunction, cytosolic mtRNA leakage and activation of the RIG-I cytosolic RNA-sensing pathway in renal tubules. Our studies suggest that RIG-I-dependent inflammation is an overlooked consequence of renal NAD^+ depletion that contributes to human KD.

Results

Altered NAD^+ metabolism is prominent in diseased human kidneys

We collected human kidney samples from healthy controls ($n = 25$) and patients with diabetic or hypertensive KD, defined as estimated glomerular filtration rate (eGFR) less than 60 ml min^{-1} per 1.73 m^2 and kidney fibrosis ($n = 25$) (Fig. 1a). The mean eGFR values were 95 ml min^{-1} per 1.73 m^2 (healthy control) and 32 ml min^{-1} per 1.73 m^2 (KD), respectively ($P < 0.001$). The demographics and clinical characteristics of the donors including eGFR, age, gender and presence of diabetes and/or hypertension are shown in Supplementary Tables 1 and 2. Using untargeted metabolomics, we identified 869 metabolites in kidney cortex lysates. Among them, 153 metabolites showed a significant ($P < 0.05$) difference (55 higher, 98 lower) in diseased kidneys (Fig. 1b and Supplementary Table 3). Elevated metabolites included urate and creatinine, well-known markers of kidney dysfunction. Next, we evaluated changes using pathway-based enrichment in MetaboAnalyst (v.5.0). We observed changes in nicotinate and NAM, pyrimidine metabolism, glycerophospholipid metabolism and histidine metabolism (Fig. 1c).

We focused on metabolites associated with nicotinate and NAM metabolism because this pathway showed the highest enrichment and had previously implicated in multiple diseases[7,8]. Levels of NAD^+, NR and NAM were lower in diseased kidneys, while NMN was not significantly changed (Fig. 1d,e). Analysis of metabolites specifically related to the de novo NAD^+ synthesis pathway revealed that the levels of quinolinate were higher in diseased kidneys, with no significant changes in tryptophan and kynurenine (Extended Data Fig. 1a,b). Notably, although the average age of patients with disease was higher than that of controls, the difference in NAD^+ metabolism remained significant ($P < 0.05$) even after downsampling to age-matched groups (Extended Data Fig. 2a,b).

To explore the underlying disease mechanisms, we conducted RNA-sequencing (RNA-seq) on kidney tissue from the same samples (Fig. 1f,g). Expression of most genes involved in NAD^+ metabolism was not consistently changed in diseased kidneys (Extended Data Fig. 1d). We next analysed genes whose expression levels correlated with tissue NAD^+ concentration. Gene ontology analysis showed enrichment for mitochondrial genes (Fig. 1g and Supplementary Table 4). Consistently, a significant correlation with kidney NAD^+ levels was observed for genes encoding mitochondrial proteins and related to mitochondrial function such as acyl-CoA dehydrogenase medium-chain (*ACADM*) (fatty acid oxidation), aconitase 2 (*ACO2*) (oxidative phosphorylation), NADH, the ubiquinone oxidoreductase core subunit V1 (*NDUFV1*) (respiration) and BCL2 associated X, BAX (apoptosis) (Fig. 1h).

Taken together, untargeted metabolomics and transcriptomics identified lower NAD^+ levels as a key feature of human KD and demonstrated a correlation between NAD^+ levels and mitochondrial gene expression.

Disturbed NAD^+ metabolism in injured mouse kidneys

Because decreases in NAD^+ were previously reported in the kidneys of mice treated with cisplatin, we next tested whether this model could broadly mimic the metabolic changes in human KD. We performed untargeted metabolomics on kidneys of wild-type (WT) mice injected with cisplatin. Kidney samples were collected 3 days after injection with phosphate-buffered saline (PBS) ($n = 4$) or cisplatin ($n = 4$). Untargeted metabolomics analysis detected 984 metabolites in kidney tissue lysates. Cisplatin injection was associated with changes in the levels of 687 metabolites ($P < 0.05$, 398 were higher and 289 were lower) (Fig. 2a,b and Supplementary Table 5). Although changes in arginine and pantothenate metabolism were more prominent in mice than in humans, consistent changes were observed in the nicotinate and NAM pathway (Fig. 2c). Kidney NAD^+ levels were dramatically lower in mice injected with cisplatin (Fig. 2d). Further mapping of the metabolites onto the NAD^+ salvage pathway showed lower levels of NR, NMN and NAM as well (Fig. 2d,e). Among metabolites in the de novo NAD^+ synthesis pathway, we observed higher levels of kynurenine and quinolinate, along with lower levels of tryptophan in kidneys of mice with cisplatin injection (Extended Data Fig. 1c). Taken together, changes in NAD^+ metabolism in injured kidneys were conserved between humans and mice.

To investigate the relationship between kidney NAD^+ levels and gene expression changes in murine kidney injury, we performed RNA-seq from the same kidney samples (Fig. 2f,g). The expression of genes involved in de novo NAD^+ synthesis, but not salvage pathway, were markedly lower in kidneys of mice receiving cisplatin injection, consistent with previous reports in injured kidneys[14]. In contrast, the mRNA expression of genes encoding many of the PARP family members, which consume NAD^+, was higher in kidneys of mice after cisplatin injection (Extended Data Fig. 1e). Similar to the human data, gene ontology analysis showed that genes whose expression levels correlated with kidney NAD^+ concentration were enriched for the mitochondrial compartment (Fig. 2g and Supplementary Table 6). In line with the human kidney data, the levels of transcripts for *Acadm*, *Aco2*, *Ndufv1* were lower, and *Bax* were higher in the kidney of cisplatin-treated mice, suggesting a link between disturbed NAD^+ metabolism and mitochondria dysfunction (Fig. 2h).

In short, integrated analysis of mouse kidney transcriptomics and metabolomics confirmed consistent changes in NAD^+ metabolism and associated gene expression signatures in injured mouse and human kidneys.

NAD^+ precursor treatment protects mice from kidney dysfunction after cisplatin injection

As we observed a markedly impaired NAD^+ metabolism in the kidneys of patients and cisplatin-injected mice, we tested whether NAD^+ precursors (NMN or NR) would protect mice from injury. Male mice were injected mice with 500 mg kg^{-1} NMN intraperitoneally for four consecutive days as described previously[22] or 435 mg kg^{-1} NR (molar equivalent). Control mice were injected with equal volume of vehicle (PBS). The first doses of NMN and NR were given 2 hours (h) before cisplatin injection, and kidneys or serum samples were collected 3 days later from each experimental group (PBS; $n = 4$, cisplatin; $n = 8$, cisplatin with NMN; $n = 8$, cisplatin with NR; $n = 8$) (Fig. 3a). Consistent with our metabolomics analysis, NAD^+ levels were lower in kidneys of mice with

https://doi.org/10.1038/s42255-023-00761-7

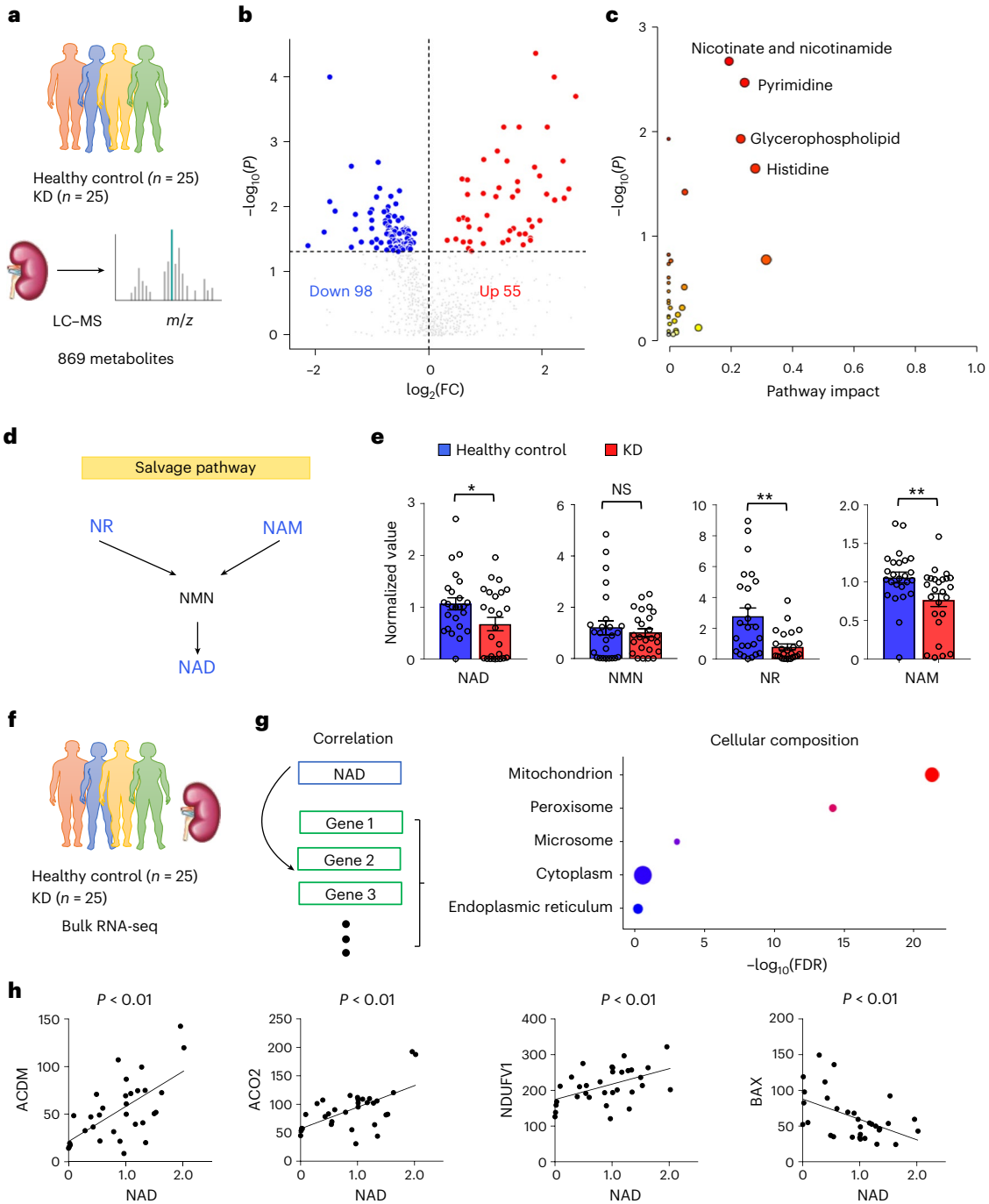

Fig. 1 | Integrated metabolomics and transcriptomics data analysis of human kidney samples. a, Total of 50 human kidney samples were collected for metabolomics analysis; including healthy controls ($n = 25$) and patients with KD ($n = 25$). **b**, Volcano plot of metabolites showing significant changes in human diseased kidneys. The x axis shows $\log_2$ fold change ($\log_2$FC). The y axis shows $-\log_{10}(P$ value). Colour indicates metabolites significantly higher (red) or lower (blue) in human diseased kidneys. Welch's two-sided t-test was used to calculate P value. **c**, Metabolic pathways showing significant changes in diseased kidneys. The dot colour indicates the level of significance, the dot size indicates pathway impact. P value was calculated from the enrichment analysis in MetaboAnalyst. **d**, The simplified NAD salvage pathway. Blue indicates metabolites significantly lower in human diseased kidneys. **e**, The levels of NAD^+, NMN, NR and NAM in human kidneys (healthy control $n = 25$ and KD $n = 25$). $^*P < 0.05$. NS, not significant. Data are presented as mean ± s.e.m. and were analysed using Welch's two-sided t-test. **f**, The bulk RNA-seq of same human kidney samples used for metabolomic studies. **g**, Gene ontology analysis of cellular composition of genes significantly correlating with kidney NAD^+ levels. The dot colour and size indicate significance and gene counts, respectively. **h**, The correlation between kidney NAD^+ levels (x axis) and relative genes expression (y axis) encoding mitochondrial proteins. P value was calculated using Pearson's correlation.

cisplatin injection (Fig. 3b). NMN or NR supplementation normalized kidney NAD^+ levels equivalently (Fig. 3b). Semiquantitative evaluation of kidney pathological specimens showed severe tubular injury represented by tubule dilation or atrophy, cast formation and epithelial cell degeneration or detachment in mice injected with cisplatin. These changes were markedly attenuated to a comparable degree in mice supplemented with NMN or NR (Fig. 3c). Serum creatinine and blood urea nitrogen (BUN) levels were elevated after cisplatin injection, and

https://doi.org/10.1038/s42255-023-00761-7

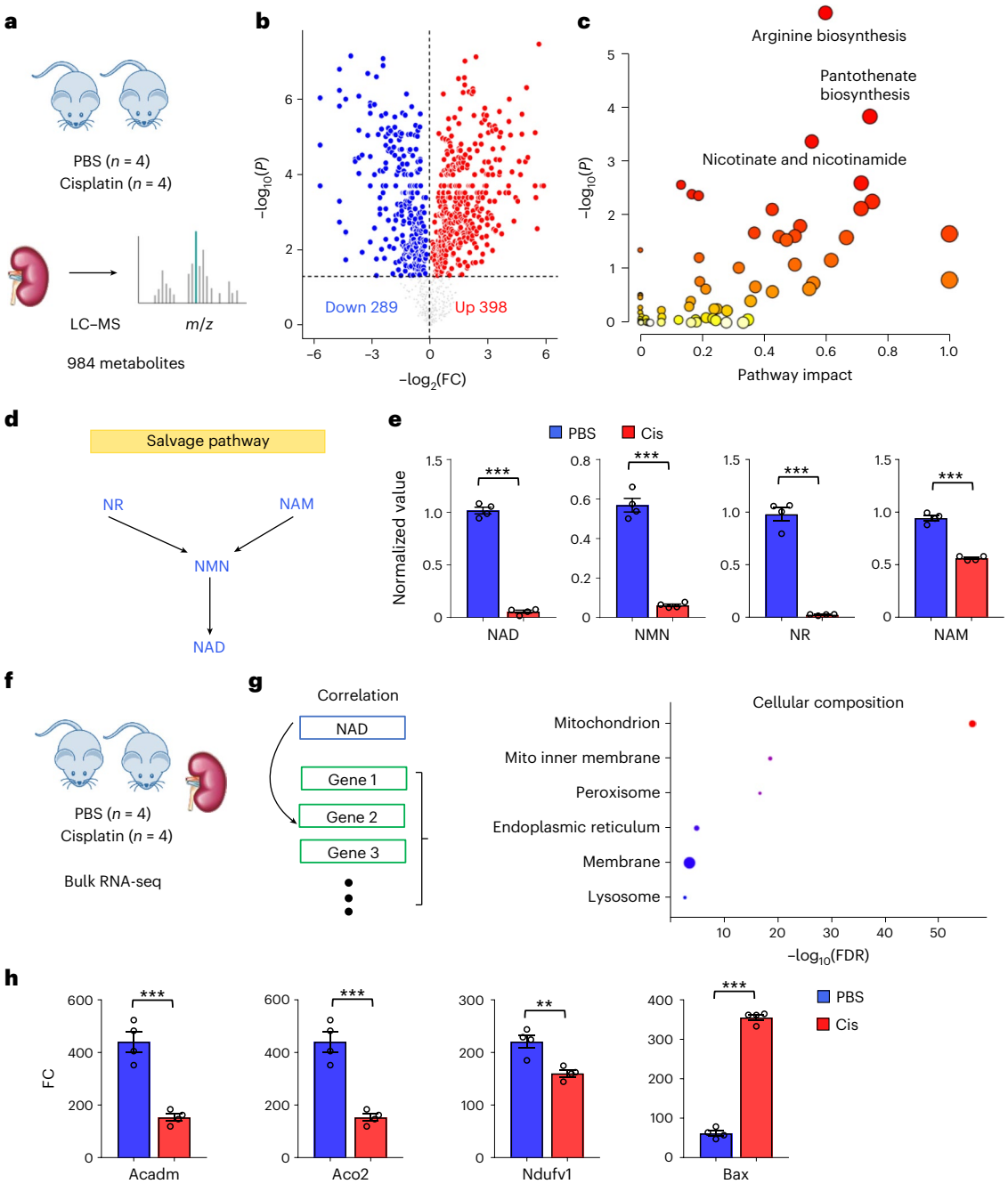

Fig. 2 | Integrated metabolomics and transcriptomics data analysis of mouse KD samples. a, Experimental set-up to collect sham (PBS, $n = 4$) or cisplatin ($n = 4$)-injected kidneys. **b**, Volcano plot showing significantly changed metabolites in the kidneys of mice. The x axis shows, $\log_2$ fold change ($\log_2$FC). The y axis shows $-\log_{10}$(P value). Colour indicates metabolites significantly higher (red) or lower (blue) in cisplatin-injected kidneys. Welch's two-sided t-test was used to calculate P value. **c**, Metabolic pathways showing significant changes in diseased kidneys. The dot colour indicates significance, the dot size indicates pathway impact. P value was calculated from the enrichment analysis in MetaboAnalyst. **d**, The salvage pathway of NAD^+ biosynthesis. Blue indicates the metabolites significantly lower in the kidneys of mice injected with cisplatin. **e**, The levels of NAD^+, NMN, NR and NAM in the kidneys of mice (PBS $n = 4$. Cis $n = 4$). $^{***}P < 0.001$. Data are presented as mean ± s.e.m. and were analysed using Welch's two-sided t-test. **f**, The bulk RNA-seq of same mice kidney samples used for metabolomics analysis. **g**, Gene ontology analysis of cellular composition of genes significantly correlated with kidney NAD^+ levels. The dot colour and size indicate significance and gene counts, respectively. **h**, The levels of *Acadm*, *Aco2*, *Ndufv1* and *Bax* in kidneys of mice (PBS $n = 4$. Cis $n = 4$). $^{***}P < 0.001$. Data are presented as mean ± s.e.m. and were analysed using a two-tailed Student's t-test.

were markedly reduced in mice supplemented with NMN or NR (Fig. 3d). Transcript levels of renal tubular injury markers, *Lcn2* (Lipocalin) and *Havcr1* (encoding KIM-1) were higher in cisplatin kidneys and reduced after NMN or NR supplementation (Fig. 3e).

Next, we sought to explore the underlying molecular mechanisms or biological pathways influenced by NAD^+ precursor supplementation. We performed bulk RNA-seq of kidneys ($n = 4$ in each experimental group). Principal components analysis (PCA) analysis showed a clear difference between groups treated with cisplatin or sham, while NMN or NR supplementation groups were more similar to the sham group (Fig. 3f). Cisplatin injection was associated with significantly higher expression of 1,762 genes and lower expression of 1,704 genes

https://doi.org/10.1038/s42255-023-00761-7

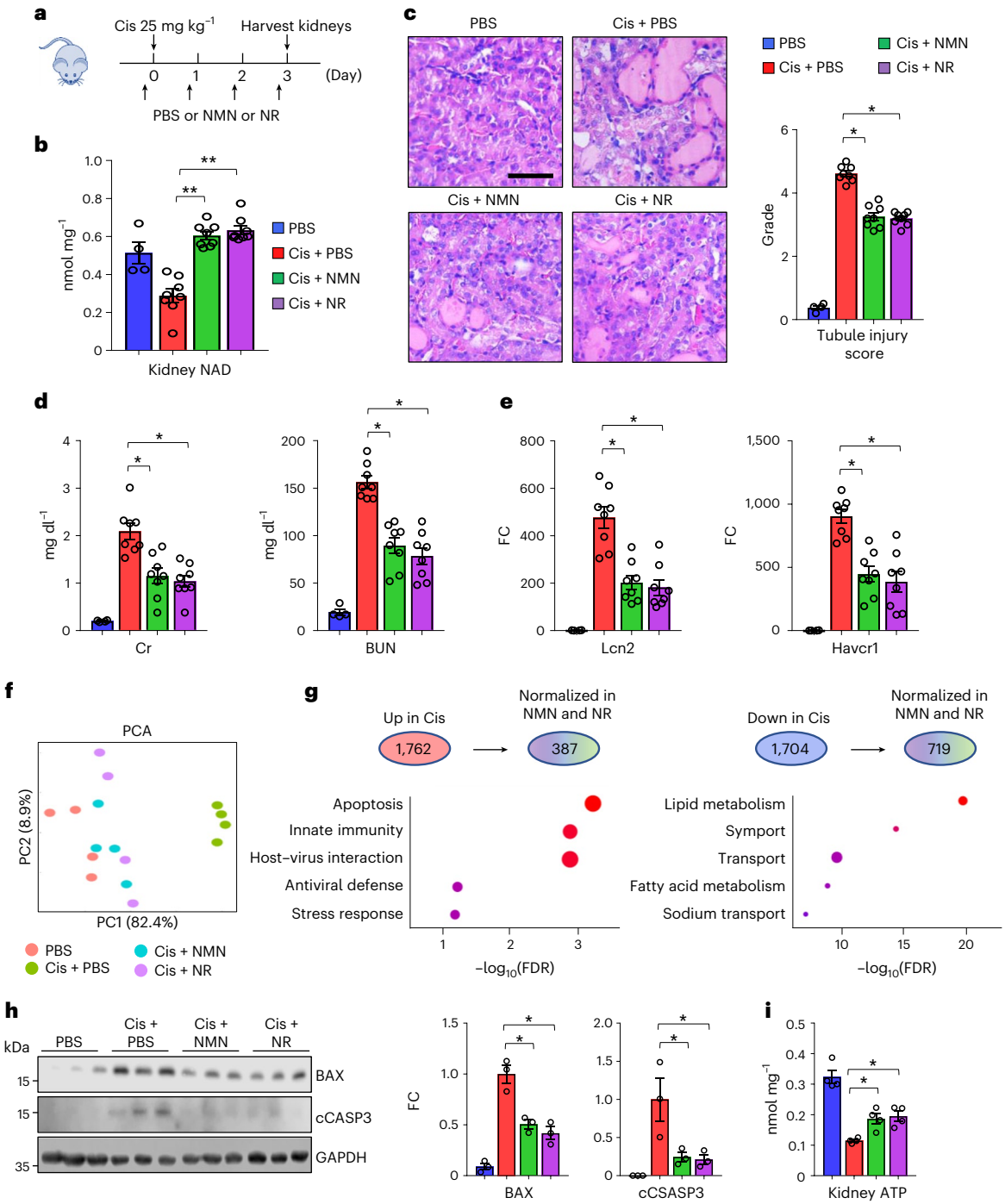

Fig. 3 | NAD⁺ precursors (NMN, NR) supplementation protected from kidney dysfunction, tubular injury and apoptosis induced by cisplatin. a, The experiment designs. NAD⁺ precursors (NMN or NR) and vehicle control (PBS) were injected i.p. for four consecutive days. The first dose was injected 2 h before cisplatin (Cis.) injection (25 mg kg^{-1}). Kidneys were collected 3 days after cisplatin injection. **b**, Kidney NAD⁺ levels in experimental groups. $^{**}P < 0.01$. **c**, Representative images of haematoxylin and eosin staining and semiquantitative analysis for tubule injury in experimental groups. Scale bars, 20 µm. $^{*}P < 0.05$. **d**, Serum creatinine and BUN levels in experimental groups. $^{*}P < 0.05$. **e**, Relative expression levels of *Lcn2* and *Havcr1* in the kidneys of mice in experimental groups. $^{*}P < 0.05$. **f**, PCA analysis of RNA-seq in experimental groups. **g**, Upper panel shows the number of genes significantly higher or lower in kidneys of mice injected with cisplatin. The number of genes normalized by both NAD⁺ precursors (NMN and NR). The lower panel shows the corresponding gene ontology analysis of normalized genes. **h**, Western blot image and quantification of BAX, cleaved caspase-3 (cCASP3) in experimental groups. The protein expression was normalized using GAPDH ($n = 3$ in each group). $^{*}P < 0.05$. **i**, Quantification of kidney ATP levels in experimental groups. The values were normalized using total protein levels ($n = 4$ in each group). $^{*}P < 0.05$. **b**–**e**, (PBS $n = 4$. Cis + PBS $n = 8$. Cis + NMN $n = 8$. Cis + NR $n = 8$). Data are presented as mean ± s.e.m. and were analysed using a one-way ANOVA followed by a Tukey post hoc test for multigroup comparison.

in kidneys when compared to sham injection (adjusted $P < 0.05$, Fig. 3g). A significant fraction (compared to random chance) returned to baseline following NMN or NR supplementation (adjusted $P < 0.05$, 387 out of 1,762 higher expressed genes, 719 genes out of 1,704 lower expressed genes). Genes normalized by NMN and NR supplementation showed enrichment for apoptosis, innate immunity and lipid

metabolism (Fig. 3g and Supplementary Tables 7 and 8). Gene ontology analysis for cellular localization indicated enrichment for mitochondria (Supplementary Fig. 1a). Consistently, the expression levels of proteins associated with intrinsic (mitochondrial) apoptosis such as BAX and cleaved caspase-3 were higher in kidneys after cisplatin injection, and their levels were reduced in NMN- or NR-treated mice (Fig. 3h). PGC1a (encoded by *Ppargc1a*) is a transcriptional coactivator that plays a dominant role in mitochondrial biogenesis and has been shown to induce NAD^+ biosynthesis via the de novo pathway[8]. NMN and NR supplementation normalized levels of *Ppargc1a* (Supplementary Fig. 1b). Kidney ATP levels were lower in all mice receiving cisplatin injection, but remained higher in mice that received NMN or NR treatment (Fig. 3g).

In summary, our results demonstrated a similar protective effect of NMN and NR on kidney function, tubule injury, tubule apoptosis and energy deficiency after cisplatin injection, while highlighting a potential role for mitochondrial pathways.

NAD^+ precursor supplementation attenuated the expression of genes associated with cytosolic RNA sensing and modulated immune cell infiltration in kidneys after cisplatin injection

Inflammation plays an important role in KD pathogenesis[23]. Gene ontology analysis revealed that genes modulated by NAD^+ replenishment were highly enriched for innate immunity and host-virus interactions (Fig. 3g). We observed that kidneys of mice with treated with cisplatin had higher expression of genes involved in cytosolic RNA sensing (*Ddx58*, *Oas1a*, *Oas1b*, *Oas1g*, *Oasl1*, *Oasl2*), and downstream interferon or nuclear factor-kB (NF-kB) signalling (*Bst2*, *Cxcl10*, *Cxcl16*, *Ifit3*, *ifitm3*, *Irf7*, *Isg15*, *Isg20*). The expression of these genes returned to baseline in mice treated with NMN or NR (Fig. 4a). Compared to its effect on *Ddx58*, cisplatin had only a modest effect on genes involved in cytosolic DNA sensing (*cGAS*, *Aim2*, *Tlr9*, *Zbp1*) (Extended Data Fig. 3a). The changes in the transcript levels of *Ddx58*, *Isg15*, *Irf7* and *Ifitm3* were validated by real-time quantitative PCR (qPCR) using different internal controls (*Gapdh*, *Actb*) (Extended Data Fig. 3b). Consistently, protein expression levels of RIG-I (encoded by *Ddx58*) were higher in kidneys with cisplatin injection, while NMN or NR treatment reduced RIG-I expression levels (Fig. 4b,c). The monomer form of MAVS did not show significant differences, but MAVS aggregation was prominent in cisplatin-treated mice and NMN or NR supplementation alleviated this aggregation (Fig. 4b,c). Because bulk RNA-seq cannot distinguish cell-type specific changes, we next isolated renal tubule cells from WT mice and incubated them with cisplatin in the presence or absence NAD^+ precursors. Cultured renal tubule cells treated with cisplatin overnight at 10 μM exhibited higher transcript expression of *Ddx58*, *Isg15*, *Irf7* and *Ifitm3*, which was partially prevented by NMN or NR supplementation (400 μM) (Fig. 4d). To further confirm the involvement of renal tubule cells in vivo, we used in situ hybridization for *Isg15* in mouse kidneys, demonstrating higher expression in cisplatin-treated mice that was lowered by NMN or NR supplementation (Fig. 4e).

Recent single-cell analyses of mouse renal disease models indicated that expression of inflammatory cytokines by kidney tubule cells could play an important role in attracting immune cells and establishing fibroinflammation[19,24]. To estimate changes in kidney immune cell populations, we used an in silico deconvolution analysis using bulk gene expression and single-cell gene marker data (Fig. 4f)[3]. Among the immune cell fraction, neutrophils, Th17, Treg and B cells were higher in kidneys after cisplatin injection, and NMN or NR supplementation reduced their numbers (Fig. 4f and Supplementary Table 9). Deconvolution analysis also showed a lower number of proximal tubule cells (including every segment: S1, S2 and S3) after cisplatin treatment, which was prevented by NMN or NR (Fig. 4f). Changes in neutrophils inferred from deconvolution analysis were validated using immunofluorescent staining of Ly6g, a surface marker of neutrophils[25]. Ly6G positive cells were higher in kidneys injected with cisplatin, and their numbers were lower after NMN or NR treatment (Fig. 4g).

Collectively, these results indicate that restoring kidney NAD^+ levels attenuated the activation of cytosolic RNA sensing and downstream inflammatory pathways and reduced immune cell infiltration in the cisplatin-induced kidney injury model.

NAD^+ precursor supplementation reduced RIG-I induction and kidney damage after ischemia-reperfusion injury (IRI)

To investigate whether effects we had observed were specific to cisplatin injury or if they reflected more general mechanisms of kidney injury, we examined the effect of NAD^+ precursor supplementation in a second KD model induced by IRI (Extended Data Fig. 4a). Kidney NAD^+ levels were decreased by IRI, and NMN and NR supplementation similarly improved kidney NAD^+ levels (Extended Data Fig. 4b). Tubule cell degeneration, detachment, tubule lumen dilation and cast formation were observed in kidneys of IRI mice. These changes were partially ameliorated by NMN and NR treatment (Extended Data Fig. 4c). Consistently, NMN and NR supplementation improved kidney function and reduced tubule injury as indicated by lower levels of Cr, BUN and expression of *Lcn* and *Havcr1* (Extended Data Fig. 4d,e). Similar to the cisplatin model, the expression of *Ddx58*, *Isg15*, *Irf7*, *ifitm3*, *Cxcl10* and *Cxcl16* were higher in IRI mice. These changes were mitigated in NMN and NR treatment (Extended Data Fig. 4f).

Collectively, NAD^+ precursor supplementation protected mice from IRI-induced kidney injury and RIG-I induction, confirming that the therapeutic benefit of NMN and NR is not limited to cisplatin-induced kidney injury.

Cisplatin-induced kidney injury leads to cytosolic leakage of mtRNA and activation of RIG-I

RIG-I (encoded by *Ddx58*) is a cytosolic RNA sensor. RIG-I is capable of detecting viral infection and activating the type 1 interferon pathway[26]. Activation of *Ddx58* is also triggered by cytosolic mtRNA release[20]. To examine changes in cytosolic mtRNA in renal tubules in response to cisplatin, we isolated cytosolic fractions from renal tubule cells, and further extracted RNA by DNase treatment (Fig. 5a). Cytosolic fractions were free of any apparent nuclear or mitochondrial contamination as indicated by the presence of glyceraldehyde 3-phosphate dehydrogenase (GAPDH) and absence of HSP60 (mitochondria), TIMM44 (mitochondria), and H3 (nuclear) (Fig. 5b). Real-time qPCR for mitochondria-specific genes (*Co2*, *Nd1*) showed that transcript levels in the cytosolic fraction were higher following cisplatin treatment, and lower following NMN or NR supplementation, indicating the leakage of mtRNA to the cytosol triggered by cisplatin was blocked with NAD^+ precursors in renal tubule cells. (Fig. 5c). RNase treatment eliminated expression of *Co2*, *Nd1*, *Nd6* and *Rnr2*, excluding of mtDNA contamination (Supplementary Fig. 2a).

To directly show the induction of *Ddx58* by cytosolic mtRNA, we next isolated mitochondria from renal tubule cells of WT mice, followed by extraction and purification of mtRNA (Fig. 5d). Then, 400 ng mtRNA was transfected to cultured renal tubule cells. Transcript levels of *Ddx58*, *Isg15*, *Irf7* and *Ifitm3* were higher in renal tubule cells 2 days after transfection with mtRNA (Fig. 5d). Notably, we did not see a significant effect on the levels of *Tmem173* (encoding the cytosolic DNA sensor STING), suggesting a minimal effect on the mtDNA sensing pathway (Fig. 5d).

We next examined whether RIG-I directly senses mtRNA. Cytosolic fraction from cisplatin-treated renal tubule cells were immunoprecipitated with RIG-I Ab or control IgG, followed by RNA extraction and purification (Fig. 5e and Supplementary Fig. 2b). Compared to control IgG Ab, RIG-I Ab extracts showed enrichment for mtRNA-encoded genes such as *Co2* and *Nd1*, indicating the direct binding of mtRNA to RIG-I (Fig. 5e).

https://doi.org/10.1038/s42255-023-00761-7

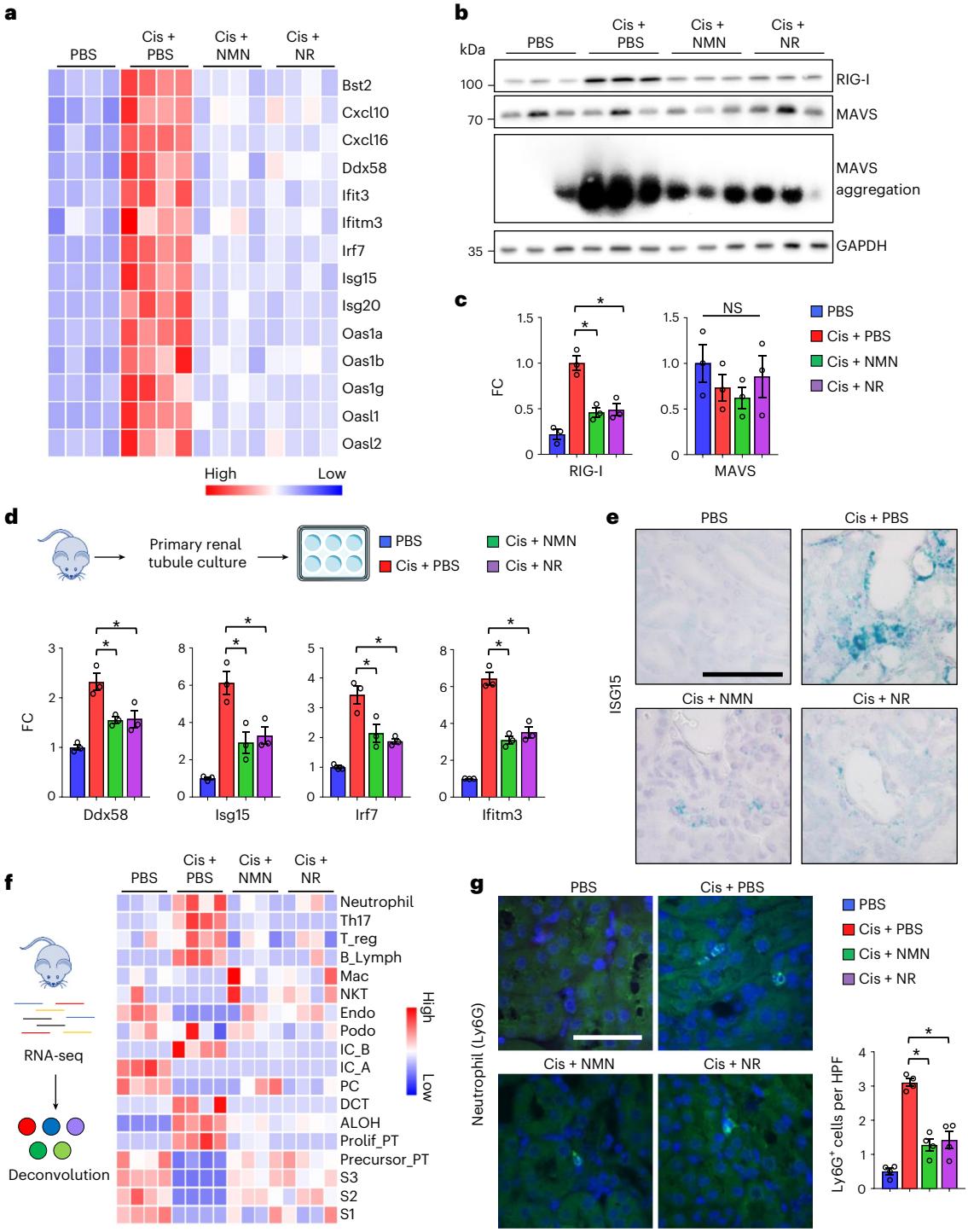

Fig. 4 | NAD⁺ precursor (NMN, NR) supplementation protected from cytosolic RNA-sensing pathway activation. a, Heatmap showing genes associated with cytosolic RNA sensing and downstream interferon stimulated genes in experimental groups. **b**, Western blot image and quantification of RIG-I, MAVS and SDD–AGE image of MAVS aggregation in the kidneys of mice in experimental groups. *$P < 0.05$. **c**, Quantification of RIG-I and MAVS in the kidneys of experimental groups ($n = 3$ in each group). *$P < 0.05$. **d**, The upper panel shows a kidney tubule cell culture from WT mice. The lower panel shows the relative transcript levels of *Ddx58*, *Isg15*, *Irf7* and *Ifitm3* in experimental groups ($n = 3$ in each group). *$P < 0.05$. **e**, The representative in situ hybridization image of *Isg15* in kidneys of mice in experimental groups. Two experiments were repeated independently. Scale bars, 20 µm. **f**, Left shows in silico cellular deconvolution analyses for the kidneys of mice in experimental groups. Right shows each row represents cell type. Colour indicates higher (red) or lower (blue) values. Mac, Macrophage; NKT, natural killer T cells; Endo, endothelial; IC, intercalated cell; PC, principal cell; DCT, distal convoluted tubule; ALOH, ascending loop of Henle and PT, proximal tubule. **g**, Representative image and quantification of neutrophil (Ly6g) staining in the kidneys of mice in experimental groups ($n = 4$ in each group). Scale bars, 20 µm. HPF, high power field. *$P < 0.05$. Data are presented as mean ± s.e.m. and were analysed using a one-way ANOVA followed by a Tukey post hoc test for multigroup comparison. Gene or protein expression levels were normalized using Gapdh.

https://doi.org/10.1038/s42255-023-00761-7

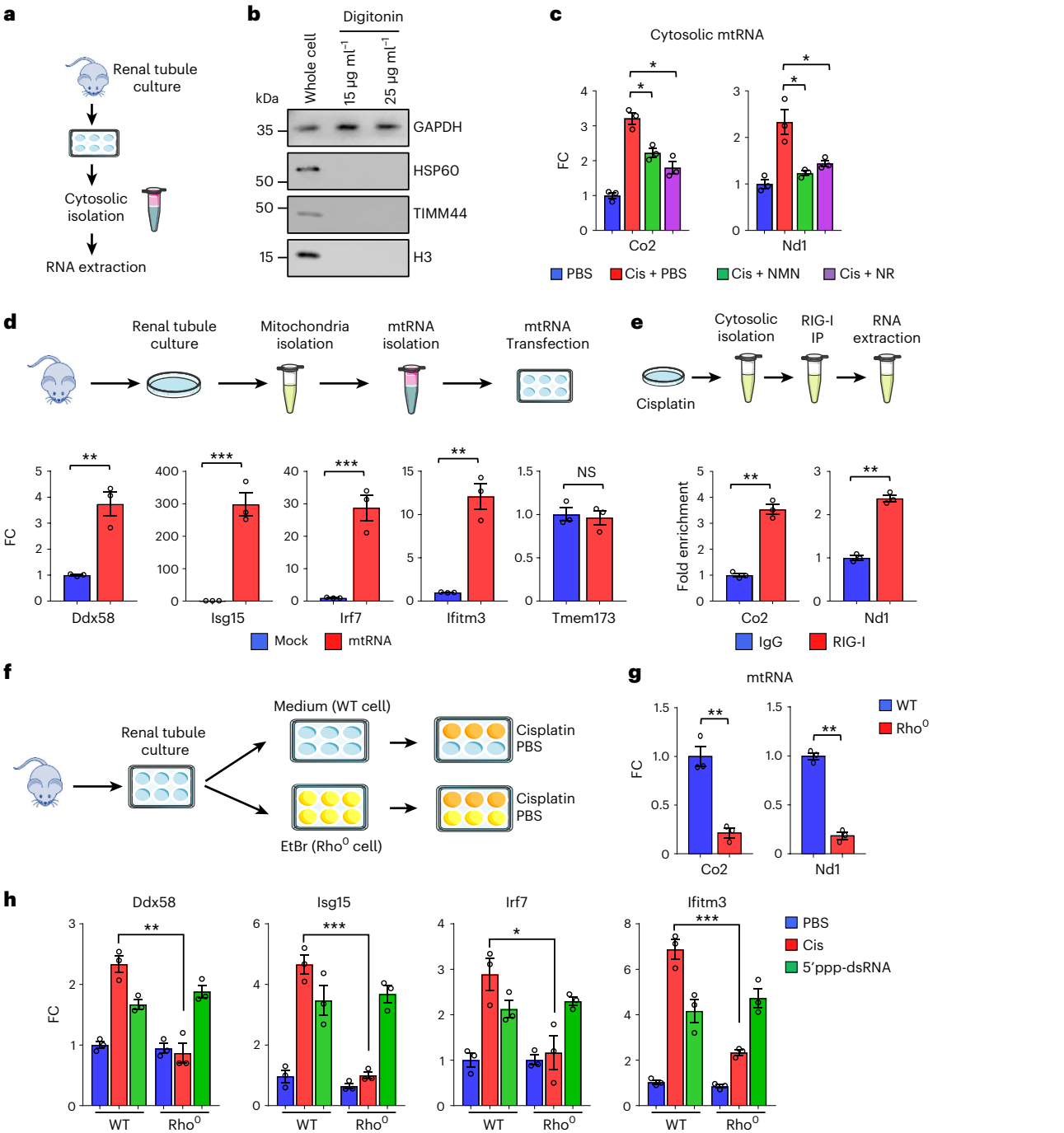

Fig. 5 | Activation of RIG-I cytosolic RNA-sensing pathway in response to cytosolic mtRNA leakage. a, Experimental design. Cytosolic RNA was isolated from cultured renal tubules of WT mice following cisplatin injury. **b**, Western blot image of GAPDH (cytosolic), HSP60 (mitochondria), TIMM44 (mitochondria) and H3 (nuclear) in whole cell or extracted cytosolic fraction using digitonin. three experiments were repeated independently. **c**, Relative transcript levels of *Co2*, *Nd1* in cytosolic fraction treated with DNase in experimental groups ($n = 3$ in each group). $^{*}P < 0.05$. **d**, Upper shows the experimental design. Extracted mtRNA was transfected to renal tubule cells. Lower shows the relative transcript levels of *Ddx58*, *Isg15*, *Irf7*, *ifitm3* and *Tmem173* in renal tubule cells treated with mock or mtRNA transfection ($n = 3$ in each group). $^{**}P < 0.01$, $^{***}P < 0.001$; NS, not significant. **e**, Experimental design. Cytosolic fraction from cisplatin-treated renal tubule cells were immunoprecipitated with RIG-I Ab or IgG, followed by RNA isolation. Fold enrichment of *Co2* and *Nd1* was calculated ($n = 3$ in each group). $^{**}P < 0.01$. **f**, Experimental design. Renal tubule cells were cultured in a medium or in the presence of EtBr (Rho^0 cells), and treated with PBS or cisplatin. **g**, Relative transcript levels of *Co2*, *ND1* in WT or Rho0 renal tubule cells. $^{**}P < 0.01$. **h**, Relative transcript levels of *Ddx58*, *Isg15*, *Irf7* and *ifitm3* in WT or Rho^0 renal tubule cells as indicated. $^{*}P < 0.05$, $^{**}P < 0.01$, $^{***}P < 0.001$. Gene expression levels were normalized using *Gapdh*. Data are presented as mean ± s.e.m. and were analysed using a two-tailed Student's *t*-test or a one-way ANOVA followed by a Tukey post hoc test for multigroup comparison.

Ethidium bromide (EtBr) depletes mtDNA without affecting nuclear DNA transcription[27]. To determine whether mtDNA/RNA-depleted cells (Rho^0 cells) are resistant to cisplatin treatment, we isolated renal tubule cells and cultured them in presence of EtBr (100 ng ml^{-1}) for 8 days (Fig. 5f). We confirmed the lack of mitochondrial DNA by negligible transcript levels of *Co2* and *Nd1* after EtBr treatment (Fig. 5g). In comparison to WT renal tubule cells, Rho^0 renal tubule cells failed to induce the expression of *Ddx58*, *Isg15*, *Irf7* and

Ifitm3 following cisplatin treatment (Fig. 5h). However, both WT and Rho^0 renal tubule cells were able to sense RNA and induce RIG-I in response to the synthetic RIG-I ligand (5′ppp-dsRNA (double-stranded RNA)) (Fig. 5h).

To directly evaluate the effect of low NAD$^+$ level on RIG-I induction, we treated tubule cells with the NAMPT inhibitor FK866 (100 nM). NAD$^+$ levels were drastically lower after 1 day of FK588 treatment (Extended Data Fig. 5a). Live cell number was unchanged on day 1 but decreased at later timepoints (Extended Data Fig. 5a). The expression levels of *Bax*, *Ddx58*, *Isg15*, *Irf7*, *Cxcl10* and *Cxcl16* were higher in NAD$^+$ depleted cells (Extended Data Fig. 5b). Restoring NAD$^+$ through NR supplementation normalized these effects (Extended Data Fig. 5b).

Collectively, these results indicate that cytosolic mtRNA leakage induced by cisplatin triggered RIG-I induction in renal tubule cells, which was prevented by NAD$^+$ precursor supplementation.

NAD$^+$ precursor supplementation prevents loss of mitochondrial activity in mouse kidneys

Cisplatin has been shown to impair mitochondrial function[28]. Having observed the protective effect of NMN and NR from cytosolic mtRNA leakage, we next examined their effects on mitochondria function in renal tubule cells. MitoSOX staining revealed higher levels of mitochondrial reactive oxygen species (mtROS) in renal tubule cells treated with cisplatin, which were reduced by NMN or NR supplementation (Fig. 6a). Mitochondrial membrane potential, evaluated by JC-1 staining, was lower in renal tubule cells treated with cisplatin, and NMN or NR supplementation equally improved mitochondrial membrane potential (Fig. 6b). Cisplatin treatment caused cell toxicity, increased *Bax* transcript levels and reduced live cell number. These changes were mitigated by NMN and NR supplementation (Fig. 6c and Extended Data Fig. 6a,b). Seahorse-based analysis of mitochondrial respiration showed overall impaired oxygen consumption rate (OCR) in renal tubule cells following cisplatin treatment and marked improvement of the maximal respiration capacity with NMN or NR supplementation (Extended Data Fig. 6c). Consistently, ATP contents in renal tubule cells were improved after NMN or NR supplementation to a similar degree (Extended Data Fig. 6d). Live cell numbers were not affected following treatment with a SIRT1 inhibitor (EX527) or a PARP1 inhibitor (Olaparib) (Extended Data Fig. 6e), suggesting that these pathways are not essential to the cisplatin-induced injury.

Next, to examine mitochondrial complex activities, we isolated mitochondria from cultured renal tubule cells. Cisplatin inhibited complex I, II and IV (CI, CII, CIV)-dependent respiration. NMN or NR supplementation improved CI activity (Fig. 6d) with a trend towards improving CII and CIV activity as well (Fig. 6d). NAD$^+$ levels in mitochondrial fractions were lower in cisplatin-treated cells, and returned to normal level following NMN or NR supplementation (Fig. 6e).

mtROS can cause apoptosis by releasing cytochrome c through BAX pores[29], which appears to regulate cytosolic mtDNA and mtRNA leakage[20]. To investigate the role of mtROS and BAX in the induction of the RIG-I cytosolic RNA-sensing pathway, we treated cultured renal tubule cells with mitoTEMPO (200 μM), or BAX inhibitor (400 μM) with or without cisplatin. Higher transcript levels of *Ddx58*, *Isg15* and *Irf7* were observed following cisplatin treatment, and these effects were attenuated in kidney tubule cells treated with mitoTEMPO or BAX inhibitor (Extended Data Fig. 7a,b).

To understand the effects of NAD$^+$ precursors on mitochondrial metabolic activity, we performed metabolomics on kidneys from the NMN- or NR-treated mice. PCA analysis showed that the NMN- and NR-treated groups clustered between sham and cisplatin groups, suggesting a partial rescue of their metabolic profiles (Fig. 6f). Among the 398 (up) and 290 (down) metabolites that showed changes in the cisplatin-injected group, 272 and 212 metabolites were normalized by NMN and NR supplementation, respectively (Fig. 6g). Most TCA cycle intermediates (citrate, aconitate, isocitric lactone, α-ketoglutarate, fumarate, malate, 2-methylcitrate) were higher in kidneys after cisplatin injection, while succinylcarnitine (C4-DC) was lower (Fig. 6h) and NMN or NR supplementation reversed most of these changes (Fig. 6i and Supplementary Table 10).

Collectively, these results indicate that NAD$^+$ precursor supplementation mitigates mitochondrial impairment induced by cisplatin in renal tubule cells and improves mitochondria metabolic activity in the kidney.

RIG-I and MAVS knock-out (KO) mice are resistant to kidney dysfunction and renal tubule injury induced by cisplatin

Because we observed changes in mtRNA release and RIG-I activation that correlated with the beneficial effects of NAD$^+$ precursors, we next sought to explore whether blocking RIG-I per se was protective against KD development. To address this, we injected WT and RIG-I KO mice with cisplatin and collected kidneys and serum samples 3 days later (Fig. 7a). Serum Cr and BUN levels, key indicators of kidney function, were improved in RIG-I KO mice compared to WT mice after cisplatin injection (Fig. 7b). Similarly, transcript levels of *Havcr1* and *Lcn2*, markers of renal tubule injury, were markedly lower in kidneys of RIG-I KO mice when compared to WT mice after cisplatin injection (Fig. 7c). Semiquantitative scoring of the renal tubule injury indicated that RIG-I KO mice had lower tubule injury compared to WT mice after cisplatin injection (Fig. 7d). As expected, RIG-I levels were markedly higher in WT mice injected with cisplatin and undetectable in RIG-I KO mice (Fig. 7e and Extended Data Fig. 8a). We found no observable changes in monomeric form of MAVS, however, MAVS aggregation was lower in cisplatin-treated RIG-I KO mice[30,31] (Fig. 7e). Levels of cleaved caspase-3, a marker of the intrinsic apoptosis pathway, were lower in RIG-I KO mice compared to WT mice (Fig. 7e, Extended Data Fig. 8a). The transcript levels of *Isg15* and *Irf7* were lower in kidneys of RIG-I KO mice treated with cisplatin (Fig. 7f) and in cisplatin-treated renal tubule cells isolated from RIG-I KO mice (Extended Data Fig. 8b). There was no observable difference in expression levels of *cGAS* and *Ifih1* in cisplatin-treated WT and RIG-I deficient renal tubule cells (Extended Data Fig. 8b), suggesting that decreased inflammatory gene expression was not due to the suppression of these alternative nucleic acid sensing pathways.

Kidney NAD$^+$ levels were lower in cisplatin-injected RIG-I KO compared to sham-treated WT or RIG-I KO mice (Extended Data Fig. 8c). NR supplementation in cisplatin-treated RIG-I deficient renal tubule cells did not further reduce the expression levels of *Isg15* and *Irf7*, indicating that the protective effect of NAD$^+$ on cisplatin-induced inflammation was mainly dependent on RIG-I (Fig. 7g).

To further examine the role of cytosolic RNA-sensing pathways in KD, we analysed MAVS KO mice following cisplatin injury (Fig. 7h). MAVS KO mice had improved kidney function and lower tubular injury, as evident by lower Cr and BUN, and lower expression of *Havcr1* and *Lcn2* (Fig. 7i,j) compared to cisplatin-treated WT mice. The expression levels of *Isg15* and *Irf7* were lower in kidney tissue and in renal tubules isolated from MAVS KO mice treated with cisplatin (Fig. 7k,l). In contrast, MDA5 deficiency had no effect on the expression of *Ddx58*, *cGAS*, *Isg15*, *Irf7* and *Ifitm3* in cisplatin-treated kidney tubule cells (Extended Data Fig. 9a).

Leakage of mtDNA in renal tubule cells treated with cisplatin has been shown to elicit inflammation via cGAS/STING[32]. Consistently, cGAS-deficient cells showed lower expression of *Isg15*, *Irf7* and *Ifitm3* in cisplatin-treated renal tubule cells. However, no change in *Ddx58* and *Ifih1* expression was observed, suggesting an independent contribution of RIG-I and cGAS to fibroinflammation and kidney injury (Extended Data Fig. 9b).

Collectively, these results confirm a role for mtRNA sensing via the RIG-I/MAVS pathway in cisplatin-induced kidney injury, as evidenced by improvement of renal function, and reduced epithelial injury and cell death in RIG-I and MAVS KO mice.

https://doi.org/10.1038/s42255-023-00761-7

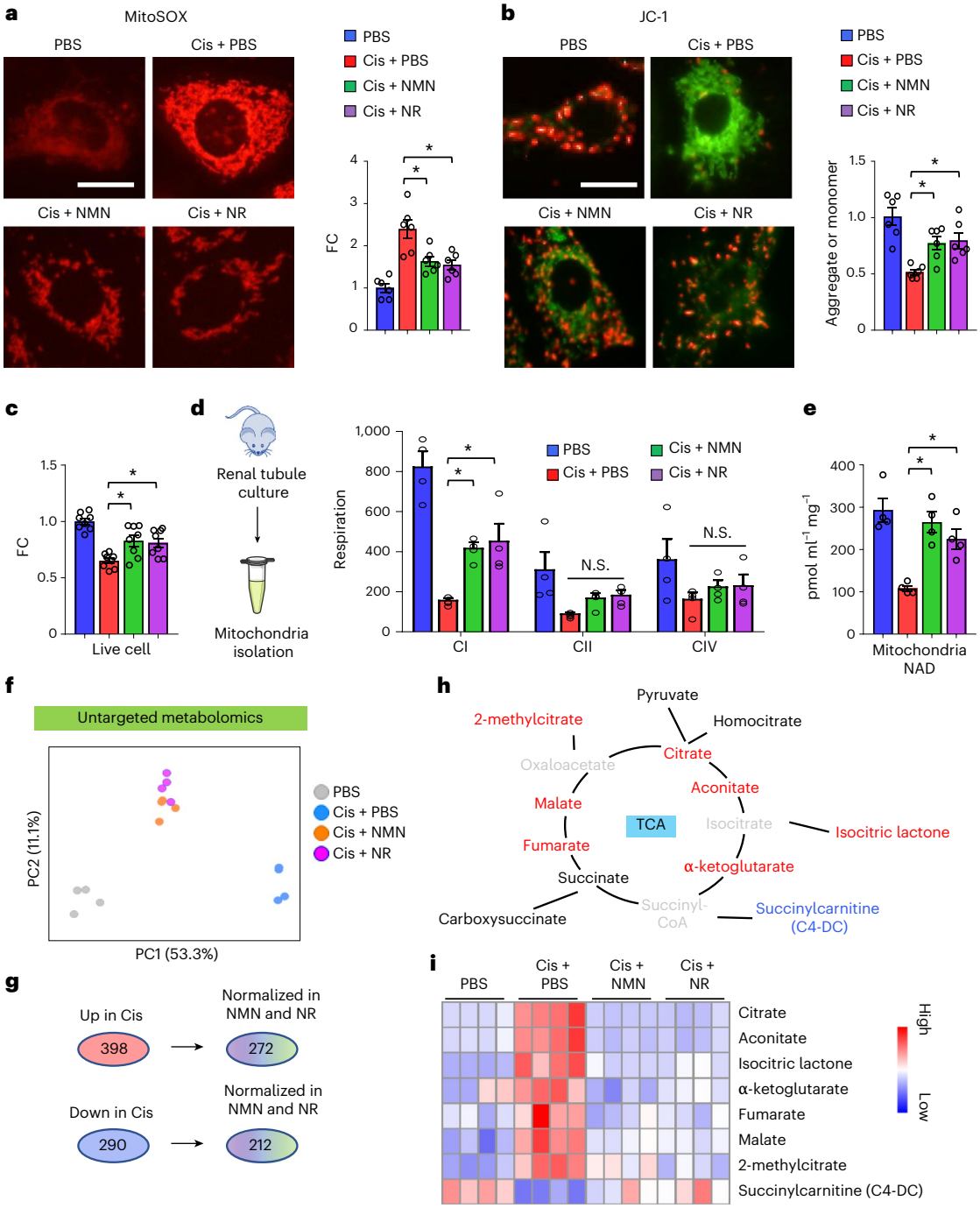

Fig. 6 | NAD⁺ precursors (NMN and NR) restored mitochondria function in renal tubule cells and mitochondrial metabolic activity in mice kidneys after cisplatin treatment. a, Representative image and quantification of MitoSOX in renal tubules in experimental groups. Scale bars, 5 μm ($n = 6$ in each group). *$P < 0.05$. **b**, Representative image and quantification of JC-1 in renal tubules in experimental groups ($n = 3$ in each group). Scale bars, 5 μm. JC-1 detect mitochondria membrane potential; aggregate form (red) and monomer form (green). *$P < 0.05$. **c**, The relative quantification of live renal tubule cells in experimental groups ($n = 8$ in each group). *$P < 0.05$. **d**, Mitochondria were isolated from cultured renal tubule cells. Mitochondria respiration in each component (CI–CIV) was monitored by Oroboros in experimental groups ($n = 3$ in each group). The values were normalized by total proteins. *$P < 0.05$. **e**, Quantification of mitochondrial NAD⁺ levels in renal tubule cells from experimental groups ($n = 4$ in each group). Values were normalized to total protein levels. *$P < 0.05$. **f**, PCA analysis of untargeted metabolomics in kidneys of mice in experimental groups. **g**, Number of metabolites significantly higher (up) or lower (down) in the kidneys of mice injected with cisplatin. Number of metabolites those levels returned to normal following NAD⁺ precursor (NMN or NR) treatment. **h**, Graphic representation of the TCA cycle intermediates. The colour indicates metabolites; significantly increased (red), decreased (blue), not changes (black), not detected (grey) in the kidneys of mice treated with cisplatin. **i**, Heatmap showing the TCA cycle intermediates and their derivative metabolites. Colour indicates higher (red) or lower (blue) levels. Data are presented as mean ± s.e.m. and were analysed using a one-way ANOVA followed by a Tukey post hoc test for multigroup comparison.

https://doi.org/10.1038/s42255-023-00761-7

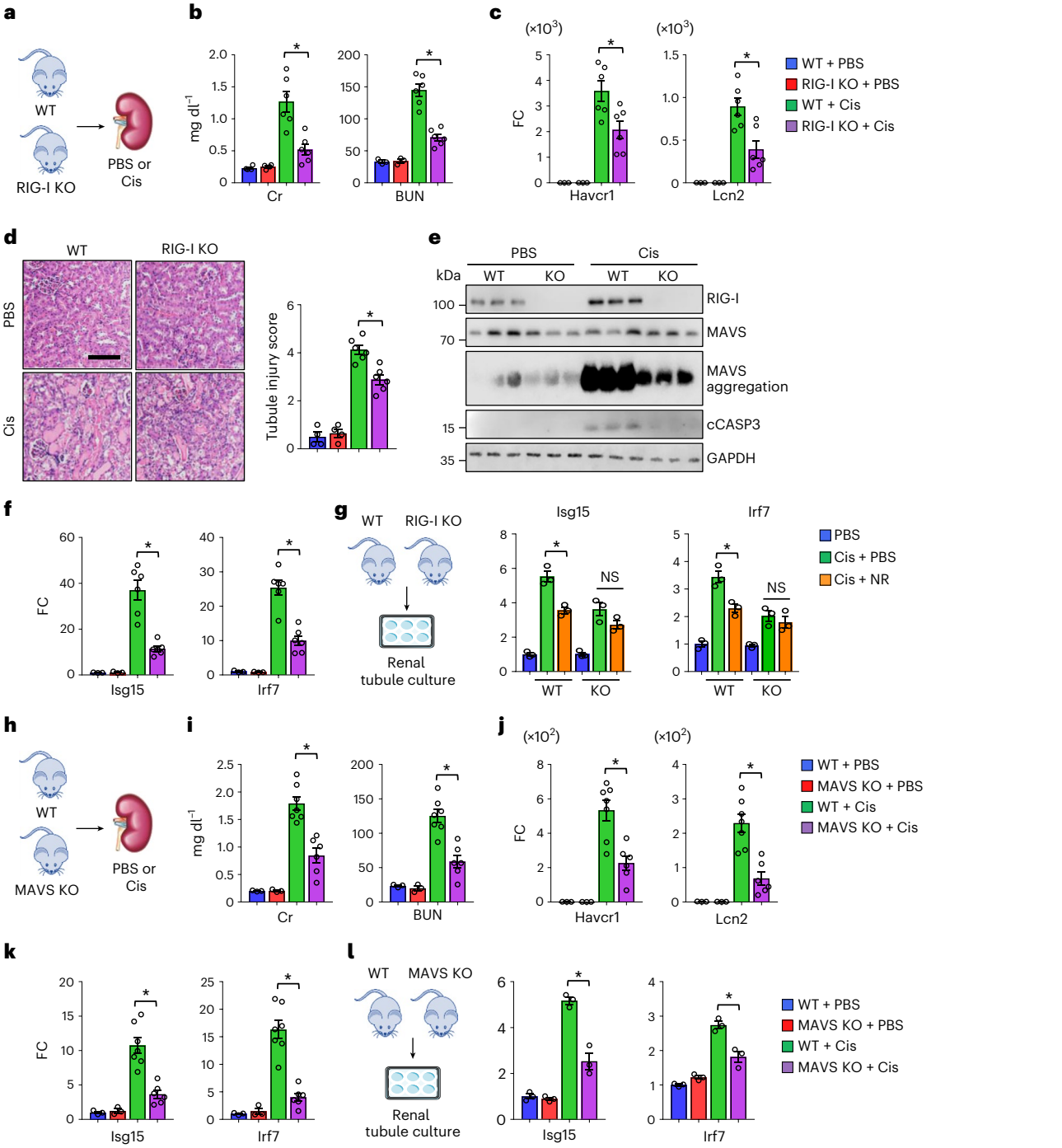

Fig. 7 | RIG-I KO and MAVS KO mice protected from kidney dysfunction, tubule injury, apoptosis induced by cisplatin. a, Experimental design. WT or RIG-I KO mice were injected with PBS or cisplatin (Cis). **b**, Serum creatinine (Cr) and BUN levels in experimental groups. *$P < 0.05$. **c**, Relative transcript levels of *Havcr1* and *Lcn2* in kidneys of experimental groups. *$P < 0.05$. **d**, Representative images of haematoxylin and eosin staining and semiquantitative analysis of renal tubule injury in experimental groups. Scale bars, 20 µm. *$P < 0.05$. **e**, Western blot image and quantification of RIG-I, MAVS, cleaved caspase-3 (cCASP3) and SDD–AGE of MAVS aggregation ($n = 3$ in each group). *$P < 0.05$, ***$P < 0.001$. NS, not significant. **f**, Relative transcript levels of *Isg15*, *Irf7* in the kidneys of experimental groups. *$P < 0.05$. **g**, Renal tubules were isolated from the kidneys of WT and RIG-I KO mice. Relative transcript levels of *Isg15*, *Irf7* in experimental groups ($n = 3$ in each group). *$P < 0.05$. **h**, Experimental design. WT and MAVS KO mice were injected with PBS or cisplatin (Cis). **i**, Serum creatinine and BUN levels in experimental groups. *$P < 0.05$. **j**, Relative transcript levels of *Havcr1* and *Lcn2* in kidneys of experimental groups. *$P < 0.05$. **k**, Relative transcript levels of *Isg15*, *Irf7* in the kidneys of experimental groups. *$P < 0.05$. **l**, Renal tubules were isolated from the kidneys of WT and MAVS KO mice. Relative transcript levels of *Isg15*, *Irf7* in experimental groups ($n = 3$ in each group). *$P < 0.05$. **b**–**d**,**f**, (WT + PBS $n = 3$. RIG-I KO + PBS $n = 3$. WT + Cis $n = 6$. RIG-I KO + Cis $n = 6$). **i**–**k** (WT + PBS $n = 3$. MAVS KO + PBS $n = 3$. WT + Cis $n = 7$. MAVS KO + Cis $n = 6$). Gene and protein expression levels were normalized using Gapdh. Data are presented as mean ± s.e.m. and were analysed using a one-way ANOVA followed by a Tukey post hoc test for multigroup comparison.

https://doi.org/10.1038/s42255-023-00761-7

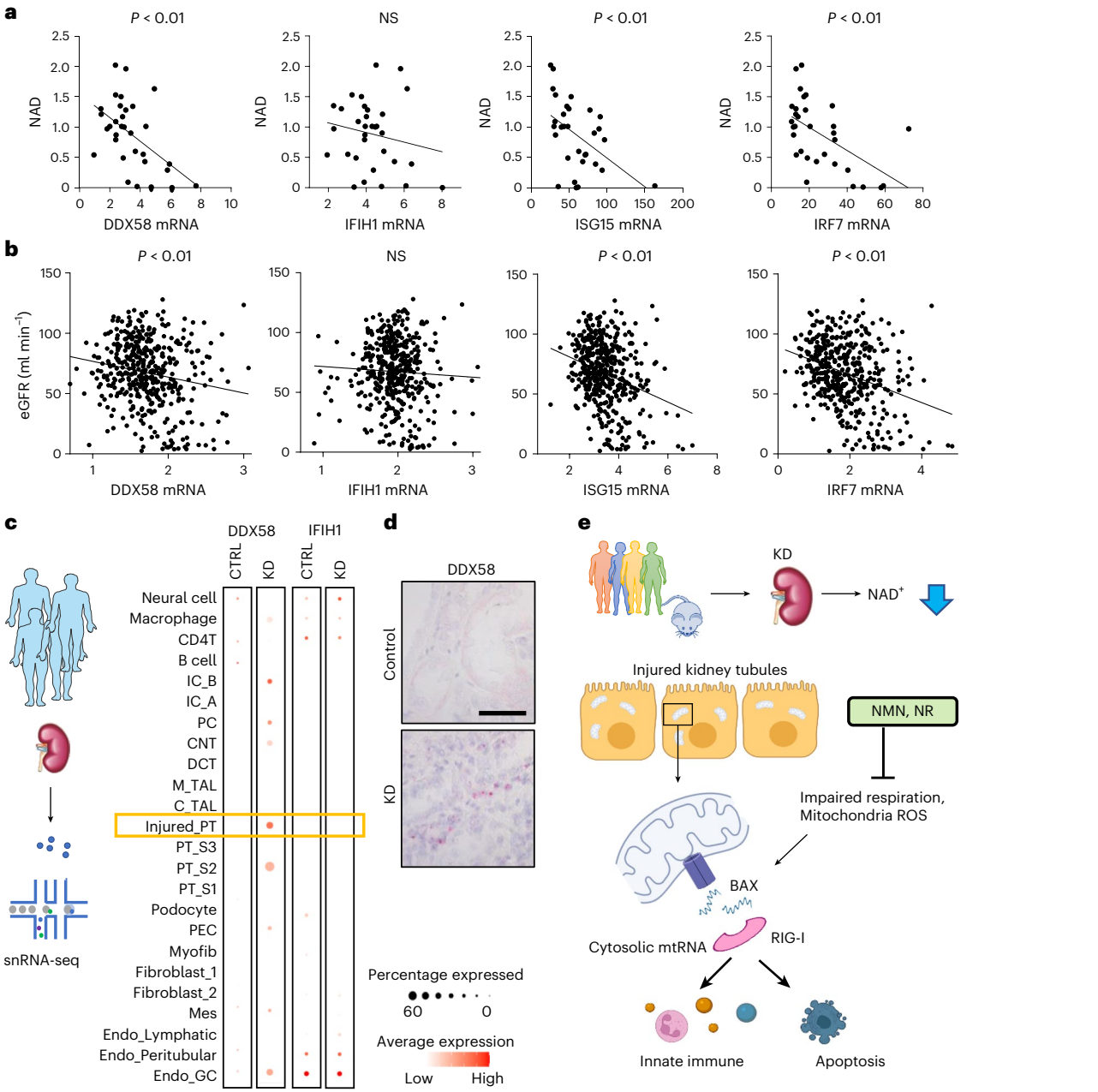

Fig. 8 | Lower NAD$^+$ levels are associated with higher RIG-I expression in renal tubules of human diseased kidneys. a, Bulk RNA-seq and untargeted metabolomics were performed in the same human kidney samples. Correlation of kidney NAD$^+$ levels and relative transcript levels of *DDX58*, *IFIH1*, *ISG15* and *IRF7*. *P* value was calculated by Pearson's correlation. **b**, The correlation of eGFR with relative transcript levels of *DDX58*, *IFIH1*, *ISG15* and *IRF7* in 432 human kidney tissue samples. The *x* axis is relative gene expression and the *y* axis is eGFR in ml min^{-1} per 1.72 m^2. *P* value was calculated by Pearson's correlation. **c**, snRNA-seq of human kidney samples. Each row represents cell type. Note that *DDX58* expression was enriched in injured proximal tubule (PT) cells in KD samples. IC, Intercalated cell; PC, principal cell; CNT, connecting tubule; DCT, distal convoluted tubule; M_TAL, thick ascending limp in the medulla; C_TAL, thick ascending limp in the cortex; PT, proximal tubule; PEC, parietal epithelial cell; MES, mesangial cell and GC, glomerular capillary. **d**, Representative image of in situ hybridization of *DDX58* in healthy control and KD samples. Scale bars, 20 µm. Two experiments were repeated independently. **e**, Proposed mechanism of proximal tubule metabolic dysfunction.

Lower NAD$^+$ levels are associated with higher RIG-I expression in renal tubules of diseased human kidneys

Our mechanistic studies using mouse kidney injury models demonstrated that NAD$^+$ precursors mitigated the activation of RIG-I-dependent cytosolic mtRNA sensing in renal tubules. Consistently, integrating transcriptomics and metabolomics information allowed us to detect a negative correlation of NAD$^+$ levels with transcript levels of *DDX58*, *ISG15* and *IRF7*, but not *IFH1* in human kidneys (Fig. 8a and Supplementary Tables 1 and 2). To further explore the association of kidney function with RIG-I-dependent cytosolic mtRNA sensing in human kidney samples, we leveraged a previously established large-scale human kidney bulk RNA-seq dataset, which included control and diseased kidneys[2] (Supplementary Table 11). Transcript levels of *DDX58*, *ISG15* and *IRF7* in human kidneys negatively correlated with eGFR and positively correlated with the degree of renal fibrosis (Fig. 8b and Extended Data Fig. 10a). The correlation of *IFIH1* expression

levels with eGFR and fibrosis was weak (Fig. 8a,b). Transcript levels of *DDX58* also positively associated with transcript levels of *ISG15*, *IRF7*, *CXCL10* and *CXCL16* in human kidneys (Extended Data Fig. 10b). Consistent with the role of PGC1α in promoting NAD^+ biosynthesis[8], *PPARGC1A* expression correlated with kidney NAD^+ levels and eGFR (Extended Data Fig. 10c). To understand cell-type specific gene expression changes, we examined single nuclear RNA-seq of human samples[33]. Single nuclear RNA-seq of diseased human kidneys showed higher expression of *DDX58*, but not *IFIH1* in injured renal tubules (Fig. 8c), which was validated by in situ hybridization (Fig. 8d).

In summary, human multi-omics data demonstrated changes consistent with mouse models, suggesting that RIG-I and cytosolic RNA-sensing are modulated by NAD^+ status and play a conserved role in human KD.

Discussion

The lack of unbiased, global human kidney metabolomics data has been a critical limitation to understanding changes in different metabolic pathways in KD. Here we analysed a mouse KD model alongside patient samples, providing a critical resource for the community. Unlike the animal models, human samples were collected mostly from patients with diabetic and hypertensive chronic kidney disease. Nevertheless, several metabolites showed consistent changes in human and murine kidneys, including those related to NAD^+ metabolism, suggesting a shared mechanism underpinning KD development independent of time course and the type of injury. Our studies indicate that kidney NAD^+ levels are regulated by both the de novo and salvage pathways, consistent with previous NAD^+ flux analysis in mice[34,35]. In contrast to de novo NAD^+ synthesis enzymes, the mRNA expression levels of NAD^+ salvage pathway enzymes were preserved in diseased kidneys from both species, suggesting that supplementation with NR or NMN is a reasonable therapeutic choice. The effectiveness of NMN and NR has rarely been compared head-to-head, but our results show that they have similar protective effects and drive comparable restoration of renal NAD^+ levels in KD models induced by cisplatin or IRI.

Mechanistically, our studies implicate the RIG-I-dependent cytosolic RNA-sensing pathway in both the underlying pathology of kidney injury and the protective effect of NAD^+ restoration. While previous studies have reported impaired NAD^+ levels in kidneys of cisplatin-treated mice, there has been no widely accepted molecular mechanism for the protection afforded by NAD^+ restoration. Leakage of mtDNA from dysfunctional mitochondria after cisplatin treatment was previously reported to activate the cytosolic DNA sensor cGAS[32], and consistently, we observed partial protection from cisplatin-induced inflammation in cGAS-depleted renal tubule cells. However, the induction of RIG-I did not require cGAS, indicating that there are independent contributions of cytosolic mtDNA and mtRNA sensing in KD[20]. Moreover, we demonstrate clear protection from cisplatin-induced injury by genetic ablation of only the mtRNA sensing pathway (RIG-I KO and MAVS KO mice) and that direct transfection of mtRNA is sufficient to induce inflammatory gene signatures that are detected in injured kidneys. Finally, we note that a hyperactivating variant of RIG-I was recently associated with kidney failure in lupus[36]. Thus, integrating unbiased transcriptomics and metabolomic data from cisplatin injury allowed us to identify a mechanism in which maintenance of renal NAD^+ levels prevents the release of mtRNA and activation of the RIG-I pathway, a prominent driver of inflammation that contributes to KD (Fig. 8e).

In conclusion, our study provides a comprehensive unbiased metabolomics dataset and highlight changes in NAD^+ metabolism in diseased human and murine kidneys. We illustrate a mechanism linking restoration of NAD^+ in renal tubules to improved mitochondrial function and attenuation of RIG-I-based cytosolic RNA sensing that drives fibroinflammation in renal tubules.

Methods

Mice

Animal studies were approved by the Institutional Animal Care and Use Committee (IACUC) of the University of Pennsylvania. WT mice were injected with cisplatin (25 mg kg^{-1}) (Cayman, no. Cay13119) dissolved in PBS intraperitoneally. To induce bilateral IRI, renal pedicles of both kidneys were exposed via dorsal incision and bilateral clamping was performed with arterial clips for 28 min. Core body temperature was measured via rectal probe and was maintained at 36.8–37.2 °C throughout the procedure using an automatic closed loop temperature control system (Homeothermic Monitoring System, Harvard Apparatus). NAD^+ precursors (NMN or NR) and vehicle control (PBS) were injected intraperitoneally for four consecutive days. The first dose was injected 2 h before cisplatin injection or IRI. The dose of NMN (500 mg kg^{-1}) were based on a previous publication[22]. The dose of NR (435 mg kg^{-1}) were calculated using the molecular ratio to generate the same amount of NAD^+ as NMN. NMN and NR were freshly dissolved in PBS on the injection day. The concentrations of NMN and NR solution were 40 and 35 mg ml^{-1}, respectively, to inject same volume. The same volume of vehicle control (PBS) was injected into control mice. Kidney and blood samples were collected 3 days after cisplatin injection or IRI surgery. RIG-I KO (stock no. 046070), MAVS KO (stock no. 008634), and MDA5 KO (stock no. 015812) mice were obtained from the Jackson Laboratory. cGAS flox mice were obtained from C. Rice (Rockefeller University)[37]. All mice were C57BL/6 background and only male mice at age 8–12 weeks were used in all experiments. Mice were housed under Specific Pathogen Free conditions with a 12-h dark/light cycle, 22–25 °C and 50–60% humidity with water and food provided ad libitum.

Sample preparation and data analysis for mice and human kidney metabolomics study

Kidneys from mice and human were collected and weighed. Snap frozen samples were sent to the Metabolon, and proceeded to measure metabolites levels in the kidneys with ultrahigh performance liquid chromatography-tandem mass spectroscopy (MS/MS). Raw data were extracted, peak-identified and quality-control processed using Metabolon's hardware and software. A data normalization step was performed to correct variation resulting from instrument inter-day tuning differences. PCA was tested to reduce the dimension of the data. The pathway analysis using MetaboAnalyst (http://www.metaboanalyst.ca) with the default setting was performed for the metabolites significantly changed in mice and human kidney tissues. The human study was deemed exempt by the Institutional Review Board of the University of Pennsylvanian as no personal identifiers were collected.

Mouse and human kidney bulk RNA-seq analysis

Total RNA was isolated from the kidneys of mice and human using the RNeasy mini kit (Qiagen no. 74126). After a sample quality check, the samples with highest RIN (RNA integrity number) were selected for library preparation. Sequencing libraries were constructed using the Illumina TruSeq RNA Preparation Kit. High-throughput sequencing was performed using Illumina NovaSeq6000 with 100 bp pair-end according to the manufacturer's instructions. Trim-galore was used to remove low-quality reads. Reads were aligned to the mouse (GRCm38) or human (hg19) reference genome using STAR (v.2.4.1d). HTSeq-0.6.1 was used for gene mapping. Differentially expressed genes between experimental groups were identified using DESeq2 v.1.10.1.

Human kidney single-nucleotide RNA-seq (snRNA-seq)

Human kidneys were homogenized and single nuclear suspension for snRNA-seq was prepared according to the manufacturer's protocol (10X Genomics)[3,38]. Quality control for constructed library was perform by Agilent Bioanalyzer High Sensitivity DNA kit. The libraries were sequenced on an Illumina HiSeq.

Estimation of cell proportions
CIBERSORTx was used to deconvolute (determine the percentage of each cell type) the bulk RNA-seq data of mouse kidney samples[39].

Western blot
Mice kidney lysates were homogenized in SDS lysis buffer (CST, no. 7722) with 2-mercaptoethanol, and boiled for 5 min at 95 °C. Lysates were transferred onto polyvinylidene difluoride membranes. After blocking in 5% milk in tris-buffered saline and 0.1% Tween-20, membranes were incubated overnight with the following antibodies at 4 °C: RIG-I (D14G6) (CST, no. 3743 S), cleaved Caspase-3 (CST, no. 9664), BAX (CST, no. 2772), MAVS (CST, no. 4983S), MDA5 (CST no. 5321) and GAPDH (CST, no. 5174). Membranes were incubated with Horseradish peroxidase-conjugated secondary antirabbit or antimouse antibody (CST no. 7074, no. 7076) for 1 h at room temperature. Signal was detected by enhanced chemiluminescence (SuperSignal West Femto Maximum Sensitivity Substrate no. 34094, Thermo Scientific). Western blots were quantified using Fiji software[40].

MAVS aggregation assay
To detect MAVS aggregation, semidenaturing detergent–agarose gel electrophoresis (SDD–AGE) was performed according to a published protocol[30]. Briefly, mitochondria fraction was isolated from mouse kidneys and resuspended in 1× sample buffer (0.5× TBE, 10% glycerol, 2% SDS and 0.0025% bromophenol blue). Samples were loaded onto a 1.5% agarose gel. After electrophoresis in running buffer (1× TBE and 0.1% SDS) for 45 min with a constant voltage of 100 V at 4 °C, the proteins were transferred to polyvinyl difluoride membrane for immunoblotting and incubated with MAVS Antibody overnight at 4 °C.

RNA immunoprecipitation assay
The cytosolic fraction isolated from cultured renal tubule cells using digitonin including RNase and protease inhibitors were treated with cisplatin for 24 h. Anti-RIG-I Ab or control IgG were added into the equally aliquoted cytosolic fractions, and gently rotated overnight at 4 °C. Protein A/G beads were then added for 2 h, followed by a washing step. RNA was extracted and purified from the precipitated samples and analysed by qPCR with reverse transcription (RT–qPCR) using mtRNA specific primers (Supplementary Table 12). Fold enrichment of mtRNA in RIG-I Ab relative to control IgG was calculated and the results of three independent experiments were plotted.

Histological analysis
Paraffin-embedded sections of mouse kidney tissue fixed in 10% formalin were cut at 5-µm thickness and deparaffinized. Haematoxylin and eosin staining and Sirius red staining (no. 24901, Polysciences) were performed according to the manufacturer's protocol. The degree of tubulointerstitial damage was scored as previously described[19]. The sections were semiquantitatively scaled (0 to 5+), according to the percentage of the area affected by hyaline casts, tubular atrophy, tubular lumen dilation and interstitial immune cells infiltration (0, normal; 1, <10%; 2, 10–25%; 3, 26–50%; 4, 51–75%; 5, >75%). Five to eight independent fields were analysed and the mean value was plotted.

For immunofluorescence staining, sections were incubated with citrate buffer at 95 °C for 10 min for antigen retrieval. Sections were allowed to cool slowly for 1 h and washed in distilled water. A non-specific signal was blocked with 10% foetal bovine serum at room temperature for 1 h. Sections were incubated overnight at 4 °C with FITC-labelled antimouse Ly6G Antibody (BioLegend, no. 127605). Sections were mounted with ProLong Gold Antifade Mountant with 4,6-diamidino-2-phenylindole (no. P36935, Invitrogen) and examined under a fluorescence microscope (OLYMPUS DP73). The Ly6G+ cells were counted in 5–8 independent fields in kidneys from each mouse ($n = 4$, each group) and the mean value was plotted.

In situ hybridization
RNAscope 2.5 HD Duplex Detection Kit (bio-techne, no. 322436) was applied to perform in situ hybridization using formalin-fixed paraffin-embedded mouse kidney tissue. The probe for human *DDX58* (Hs-RIG-I-C2 no. 550261) and mice *Isg15* (Mm-Isg15-O1 no. 559271) were used for the RNAscope assay.

RT–qPCR
RNA was isolated from kidney tissue or cells using Trizol (Invitrogen no. 15596018) or RNeasy mini kit (Qiagen no. 74106). RNA was reverse transcribed using the High-Capacity complementary DNA Reverse Transcription Kit (Applied Biosystems no. 4368813) and RT–qPCR was run in the ViiA 7 System (Life Technologies) instrument using SYBR Green Master Mix (Applied Biosystems no. 4367659) and gene-specific primers. For quantitative analysis, samples were normalized using GAPDH or ACTB with the delta delta CT method. Primer sequences are listed in Supplemental Table 12.

In vitro experiments using renal tubule cells
Renal tubule cells were isolated from 3 to 4 weeks old WT or RIG-I KO mice. Kidneys were minced and incubated for 30 min at 37 °C with collagenase I (Worthington Biochemical Product no. CLS-1). Digested kidney cells were filtered through the 100, 70 and 40 µm mesh. Cell suspensions were cultured in Roswell Park Memorial Institute (RPMI) medium 1640 (Corning no. 10-040-CM) supplemented with 10% foetal bovine serum (Atlanta Biologicals no. S11950), 20 ng ml^{-1} EGF (Peprotech no. AF-100-15), ITS (Gibco no. 51500–056) and 1% penicillin-streptomycin (Corning no. 30-002-CI) at 5% CO_2 and 37 °C.

Renal tubule cells were treated with cisplatin (10 µM) or PBS overnight. NAD^+ precursors (400 µM, NMN, NR), mitoTEMPO (200 µM, Sigma, no. SML0737), BAX inhibitor (400 µM, Cayman Chemical no. 30243), EX527 (10 µM, SIRT1 inhibitor, Sigma no. E7034), Olaparib (10 µM, PAPR inhibitor, Selleck Chemicals, no. S1060) and their vehicle controls were supplemented 2 h before cisplatin treatment. Renal tubule cells were incubated with FK866 (100 nM, NAMPT inhibitor, Cayman Chemical, no. 13287) to delete NAD^+ for indicated time. mtROS and membrane potential were assessed by staining MitoSOX (Thermo, no. M36008) and JC-1 (Thermo, no. T3168), respectively, according to the manufacturer's instructions. The fluorescent signal was measured by microplate reader for quantification. Live cells assay (Promega; no. G9200), cytotoxicity assay (Promega; no. G17800) and ATP contents measurement (Biovision; no. K354) were tested according to the manufacturer's instructions.

Renal tubule cells isolated from cGAS flox/flox mice were transfected with green fluorescent protein-Cre (GFP-Cre) or GFP adenovirus. After 48 h of incubation, renal tubule cells were treated with 10 µM cisplatin for 24 h.

Mitochondrial isolation from renal tubule cells
Cultured renal tubules were dissociated using trypsin, washed with PBS and centrifuged at 500*g* at 4 °C for 10 min. Samples were resuspended in mitochondrial isolation buffer (containing 210 mM mannitol, 70 mM sucrose, 1 mM EDTA, 10 mM HEPES, final pH adjusted to 7.2) with 0.25% fatty acid-free bovine serum albumin. Samples were homogenized using an IKA RW20 digital homogenizer at 12,000 rpm per min 20 times at cold room[41]. Samples were centrifuged at 800*g* for 5 min at 4 °C. The supernatant containing mitochondria was transferred to the new tubes, and then centrifuged at 10,000*g* for 10 min at 4 °C. The pelleted mitochondrial fraction was collected and used for downstream assay.

Oxygen consumption measurements in renal tubule cells
For real-time analysis of the OCR, renal tubule cells were analysed using an XF-96 Extracellular Flux Analyzer (Seahorse Bioscience). In brief, cells were plated in XF-96 cell culture plates, and treated with PBS or cisplatin with or without NAD^+ precursors (NMN, NR).

The following substrates were used to estimate OCR: 1 µM oligomycin, 1.5 µM fluoro-carbonyl cyanide phenylhydrazone and 100 nM rotenone plus 1 µM antimycin A.

In vitro mitochondria high-resolution respiration assay in renal tubule cells

The activity of complex I, II and IV in mitochondria of renal tubule cells was examined using Oroboros Instruments. Briefly, 200 µg mitochondria were resuspended in the respiration buffer, containing 110 mM mannitol, 0.5 mM EGTA, 3 mM $MgCl_2$, 20 mM taurine, 10 mM KH2PO4, 60 mM K lactobionate, 0.3 mM DTT and 0.1% fatty acid-free bovine serum albumin at pH 7.2 (ref. [41]). After measuring baseline OCR, oxygen concentration were continuously recorded. Complex I-dependent respiration was induced by adding 10 mM pyruvate, 10 mM malate and 1 mM ADP. An inhibitor of Complex I, rotenone (0.5 µM), was used to determine Complex I-dependent respiration. Antimycin A (5 µM) was used to inhibit complex III, followed by TMPD (0.5 mM) and ascorbate (2 mM) as artificial substrates for complex IV[41]. The data were analysed using DatLab software v.4.3 (Oroboros Instruments).

NAD measurement of mitochondria

NAD in the isolated mitochondria from renal tubule cells were measured by an enzymatic cycling assay in a 96-well format as previously described[41]. The concentration of NAD was determined by measuring the rate of resorufin accumulation in microplate reader with fluorescence excitation at 544 nm and emission at 590 nm (ref. [41]). The values were normalized by total protein levels.

Cytosolic extraction from renal tubule cells

Cytosolic fraction was extracted as described previously[21]. Renal tubule cells were resuspended in roughly 500 µl buffer containing 150 mM NaCl, 50 mM HEPES pH 7.4 and 15–25 µg ml^{-1} digitonin (no. 300410 Millipore). Samples were incubated for 10 min at 4 °C with constant rotation to allow selective plasma membrane permeabilization, followed by centrifuge at 980*g* for 10 min at 4 °C. The cytosolic supernatants were transferred to fresh tubes and centrifuged at 17,000*g* for 10 min to remove cellular debris, mitochondria and nuclei. Purity of cytosolic fraction was examined by western blot analysis.

The evaluation of cytosolic mtRNA expression in renal tubule cells

Cytosolic fractions from kidney tubules were extracted as described previously[20]. Briefly, PBS resuspended cells were aliquoted equally to two tubes. The first tube was used to extract the cytosolic fraction. The second tube was used for normalization. RNA was extracted and purified in both tubes using RNA extraction kit (no. 74106, Qiagen) with optional DNase treatment (no. 79254, Qiagen) according to the manufacturer's protocol. Equal volumes of eluate were used for cDNA production. Samples were optionally incubated with RNase A (CST, no. 7013) at 100 µg ml^{-1}, 37 °C for 30 min. Mitochondrial gene transcripts in the cytosolic fraction were evaluated by real-time qPCR using mitochondrial genome specific primers (Supplementary Table 12). RT–qPCR was run in the ViiA 7 System (Life Technologies) instrument using SYBR Green Master Mix (Applied Biosystems no. 4367659).

Transfection of mitochondria RNA into renal tubule cells

Here, 400 ng isolated mitochondria were transfected into renal tubule cells using lipofectamine 3000 (Thermo, no. L3000008). Total RNA was corrected 24 h after transfection from renal tubule cells.

Establishment of Rho^0 renal tubule cells

Renal tubule cells were cultured in RPMI medium in presence of EtBr (100 ng ml^{-1}), uridine (50 µg ml^{-1}) and sodium pyruvate (1 mM) for 8 d to make mtDNA- or mtRNA-depleted cells. The loss of mtRNA was confirmed by qPCR. No apparent cell death was observed following EtBr treatment, however, cell growth was slower compared to untreated cells. Both untreated and Rho^0 cells were treated with cisplatin when cells reached to 80 to 90% confluency. Then 500 ng RIG-I agonist (5′ppp-dsRNA #tlrl-3prna, Invivogen) were transfected into Rho^0 cells as a positive control.

Statistics

All data are shown as mean ± s.e.m. Comparisons between two groups were analysed using unpaired two-tailed Student's *t*-test. Comparisons between three or more groups were analysed using one-way analysis of variance (ANOVA) followed by Tukey's post hoc testing. For metabolomics data, Welch's two-sample *t*-test was used. A *P* value of less than 0.05 was considered significant.

Study approval

All animal work was performed in accordance with the guidelines and with approval of the University of Pennsylvania IACUC.

Reporting summary

Further information on research design is available in the Nature Portfolio Reporting Summary linked to this article.

Data availability

Gene expression data in this paper are deposited to GSE207587. The RNA-seq data for large-scale human kidney samples are available in GSE115098. Source data are provided with this paper.

References

1. Doke, T. et al. Transcriptome-wide association analysis identifies DACH1 as a kidney disease risk gene that contributes to fibrosis. *J. Clin. Investig.* **131**, e141801 (2021).
2. Qiu, C. et al. Renal compartment-specific genetic variation analyses identify new pathways in chronic kidney disease. *Nat. Med.* **24**, 1721–1731 (2018).
3. Sheng, X. et al. Mapping the genetic architecture of human traits to cell types in the kidney identifies mechanisms of disease and potential treatments. *Nat. Genet.* **53**, 1322–1333 (2021).
4. Liu, B. C., Tang, T. T., Lv, L. L. & Lan, H. Y. Renal tubule injury: a driving force toward chronic kidney disease. *Kidney Int.* **93**, 568–579 (2018).
5. Nadour, Z. et al. Validation of a liquid chromatography coupled to tandem mass spectrometry method for simultaneous quantification of tryptophan and 10 key metabolites of the kynurenine pathway in plasma and urine: application to a cohort of acute kidney injury patients. *Clin. Chim. Acta; Int. J. Clin. Chem.* **534**, 115–127 (2022).
6. Xu, J., Kitada, M. & Koya, D. NAD(+) homeostasis in diabetic kidney disease. *Front. Med.* **8**, 703076 (2021).
7. Ralto, K. M., Rhee, E. P. & Parikh, S. M. NAD(+) homeostasis in renal health and disease. *Nat. Rev. Nephrol.* **16**, 99–111 (2020).
8. Tran, M. T. et al. PGC1α drives NAD biosynthesis linking oxidative metabolism to renal protection. *Nature* **531**, 528–532 (2016).
9. Jia, Y. et al. Nicotinamide mononucleotide attenuates renal interstitial fibrosis after AKI by suppressing tubular DNA damage and senescence. *Front. Physiol.* **12**, 649547 (2021).
10. Morevati, M. et al. Effect of NAD^+ boosting on kidney ischemia-reperfusion injury. *PLoS ONE* **16**, e0252554 (2021).
11. Myakala, K. et al. NAD metabolism modulates mitochondrial function and inflammation and prevents progression of diabetic kidney disease. https://www.biorxiv.org/content/10.1101/2021.12.05.471273v2 (2021).
12. Zheng, M. et al. Nicotinamide reduces renal interstitial fibrosis by suppressing tubular injury and inflammation. *J. Cell. Mol. Med.* **23**, 3995–4004 (2019).

13. Liu, X. et al. Impaired nicotinamide adenine dinucleotide biosynthesis in the kidney of chronic kidney disease. *Front. Physiol.* **12**, 723690 (2021).
14. Poyan Mehr, A. et al. De novo NAD(+) biosynthetic impairment in acute kidney injury in humans. *Nat. Med.* **24**, 1351–1359 (2018).
15. Raines, N. H. et al. Niacinamide may be associated with improved outcomes in COVID-19-related acute kidney injury: an observational study. *Kidney360* **2**, 33–41 (2021).
16. Simic, P. et al. Nicotinamide riboside with pterostilbene (NRPT) increases NAD(+) in patients with acute kidney injury (AKI): a randomized, double-blind, placebo-controlled, stepwise safety study of escalating doses of NRPT in patients with AKI. *BMC Nephrol.* **21**, 342 (2020).
17. Yoshino, J., Baur, J. A. & Imai, S. I. NAD(+) intermediates: the biology and therapeutic potential of NMN and NR. *Cell Metab.* **27**, 513–528 (2018).
18. Martin, D. R., Lewington, A. J., Hammerman, M. R. & Padanilam, B. J. Inhibition of poly(ADP-ribose) polymerase attenuates ischemic renal injury in rats. *Am. J. Physiol. Regulatory, Integr. Comp. Physiol.* **279**, R1834–R1840 (2000).
19. Doke, T. et al. Single-cell analysis identifies the interaction of altered renal tubules with basophils orchestrating kidney fibrosis. *Nat. Immunol.* **23**, 947–959 (2022).
20. Tigano, M., Vargas, D. C., Tremblay-Belzile, S., Fu, Y. & Sfeir, A. Nuclear sensing of breaks in mitochondrial DNA enhances immune surveillance. *Nature* **591**, 477–481 (2021).
21. Dhir, A. et al. Mitochondrial double-stranded RNA triggers antiviral signalling in humans. *Nature* **560**, 238–242 (2018).
22. Guan, Y. et al. Nicotinamide mononucleotide, an NAD(+) precursor, rescues age-associated susceptibility to AKI in a sirtuin 1-dependent manner. *J. Am. Soc. Nephrology* **28**, 2337–2352 (2017).
23. Rabb, H. et al. Inflammation in AKI: current understanding, key questions, and knowledge gaps. *J. Am. Soc. Nephrology* **27**, 371–379 (2016).
24. Kirita, Y., Wu, H., Uchimura, K., Wilson, P. C. & Humphreys, B. D. Cell profiling of mouse acute kidney injury reveals conserved cellular responses to injury. *Proc. Natl Acad. Sci. USA* **117**, 15874–15883 (2020).
25. Hasenberg, A. et al. Catchup: a mouse model for imaging-based tracking and modulation of neutrophil granulocytes. *Nat. Methods* **12**, 445–452 (2015).
26. Rehwinkel, J. & Gack, M. U. RIG-I-like receptors: their regulation and roles in RNA sensing. *Nat. Rev. Immunol.* **20**, 537–551 (2020).
27. Desjardins, P., Frost, E. & Morais, R. Ethidium bromide-induced loss of mitochondrial DNA from primary chicken embryo fibroblasts. *Mol. Cell. Biol.* **5**, 1163–1169 (1985).
28. Kleih, M. et al. Direct impact of cisplatin on mitochondria induces ROS production that dictates cell fate of ovarian cancer cells. *Cell Death Dis.* **10**, 851 (2019).
29. Redza-Dutordoir, M. & Averill-Bates, D. A. Activation of apoptosis signalling pathways by reactive oxygen species. *Biochim. Biophys. Acta* **1863**, 2977–2992 (2016).
30. Hou, F. et al. MAVS forms functional prion-like aggregates to activate and propagate antiviral innate immune response. *Cell* **146**, 448–461 (2011).
31. Liu, S. et al. Phosphorylation of innate immune adaptor proteins MAVS, STING, and TRIF induces IRF3 activation. *Science* **347**, aaa2630 (2015).
32. Maekawa, H. et al. Mitochondrial damage causes inflammation via cGAS-STING signaling in acute kidney injury. *Cell Rep.* **29**, 1261–1273.e1266 (2019).
33. Abedini, A. et al. Spatially resolved human kidney multi-omics single cell atlas highlights the key role of the fibrotic microenvironment in kidney disease progression. https://www.biorxiv.org/content/10.1101/2022.10.24.513598v1 (2022).
34. McReynolds, M. R. et al. NAD(+) flux is maintained in aged mice despite lower tissue concentrations. *Cell Syst.* **12**, 1160–1172. e1164 (2021).
35. Liu, L. et al. Quantitative analysis of NAD synthesis-breakdown fluxes. *Cell Metab.* **27**, 1067–1080.e1065 (2018).
36. Peng, J. et al. Clinical implications of a new DDX58 pathogenic variant that causes lupus nephritis due to RIG-I hyperactivation. *J. Am. Soc. Nephrol.* **34**, 258–272 (2022).
37. Schoggins, J. W. et al. Pan-viral specificity of IFN-induced genes reveals new roles for cGAS in innate immunity. *Nature* **505**, 691–695 (2014).
38. Doke, T. et al. Genome-wide association studies identify the role of caspase-9 in kidney disease. *Sci. Adv.* **7**, eabi8051 (2021).
39. Steen, C. B., Liu, C. L., Alizadeh, A. A. & Newman, A. M. Profiling cell type abundance and expression in bulk tissues with CIBERSORTx. *Methods Mol. Biol.* **2117**, 135–157 (2020).
40. Schindelin, J. et al. Fiji: an open-source platform for biological-image analysis. *Nat. Methods* **9**, 676–682 (2012).
41. Mukherjee, S. et al. SIRT3 is required for liver regeneration but not for the beneficial effect of nicotinamide riboside. *JCI Insight* **6**, e147193 (2021).

Acknowledgements

This work has been supported by the National Institute of Health, in the Susztak laboratory grant nos. NIH R01 DK087635, DK076077 and DK105821 and in the Baur laboratory by grant nos. DK098656 and HL165792. Additional funding and research materials were provided by Metro International Biotech through a sponsored research agreement to J.A.B. and K.S. We thank the Molecular Pathology and Imaging Core (grant no. P30-DK050306) and the Diabetes Research Center (grant nos. P30-DK19525 and S10 OD025098) at University of Pennsylvania for their services.

Author contributions

This study was led by K.S. with assistance from J.A.B. These authors jointly supervised this work. T.D. performed experiments with assistance from S.M., D.M., K.C., J.G.D., B.C., A.A. and P.D. T.D., J.A.B. and K.S. wrote the manuscript.

Competing interests

Work in the Susztak laboratory is supported by Gilead, GSK, Boehringer, Regeneron, Novo Nordisk, Novartis, Calico, Astra Zeneca, Genentech, Ventus and Maze Biotech. J.A.B. is consultant to Pfizer and Cytokinetics, an inventor on a patent for using NAD^+ precursors in liver injury and has received research funding and materials from Elysium Health and Metro International Biotech, both of which have an interest in NAD^+ precursors. The other authors declare no competing interests.

Additional information

Extended data is available for this paper at https://doi.org/10.1038/s42255-023-00761-7.

Supplementary information The online version contains supplementary material available at https://doi.org/10.1038/s42255-023-00761-7.

Correspondence and requests for materials should be addressed to Joseph A. Baur or Katalin Susztak.

Peer review information *Nature Metabolism* thanks Hiroshi Itoh and the other, anonymous, reviewer(s) for their contribution to the peer review of this work. Primary Handling Editor: Isabella Samuelson, in collaboration with the *Nature Metabolism* team.

https://doi.org/10.1038/s42255-023-00761-7

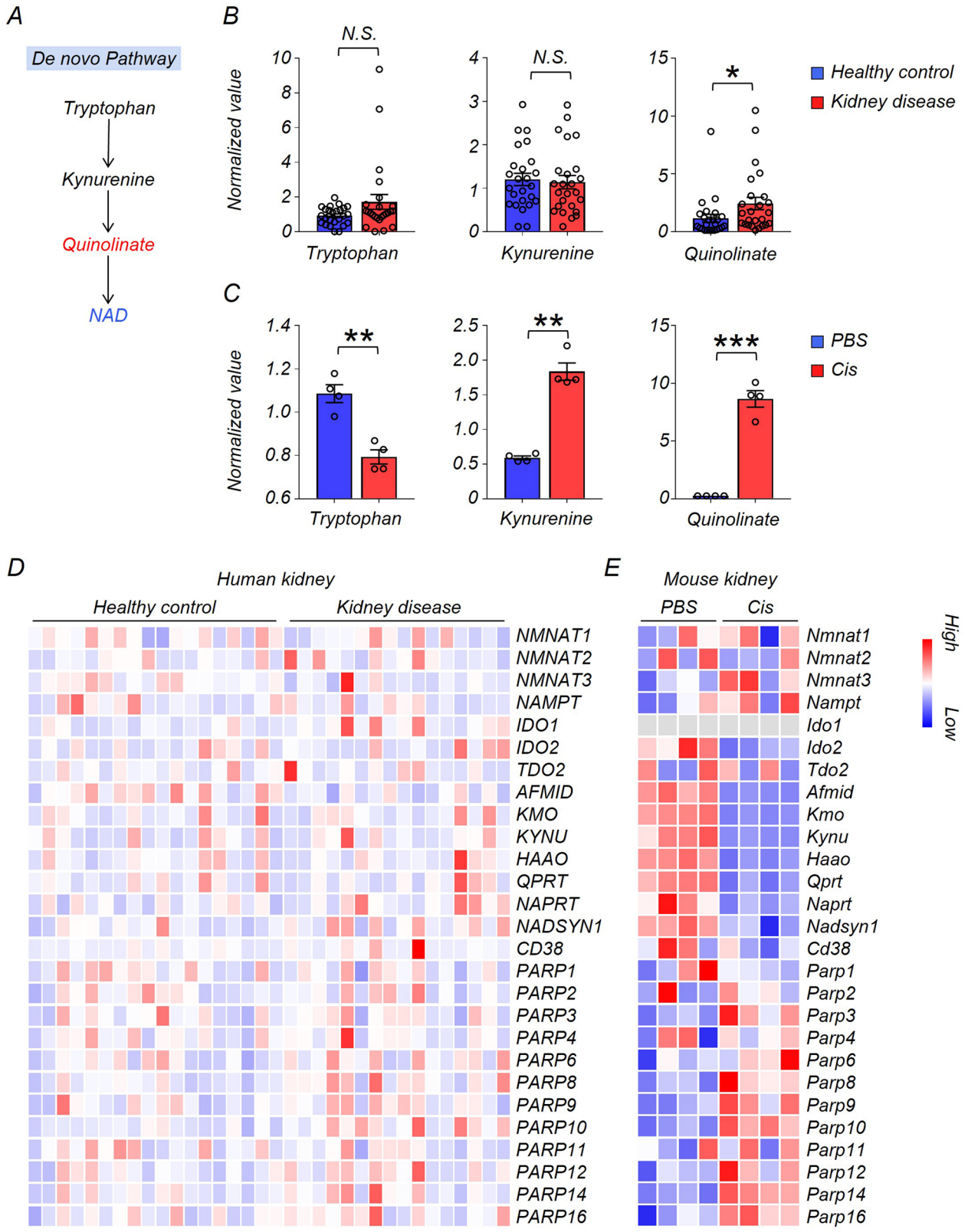

Extended Data Fig. 1 | Changes in de novo NAD$^+$ synthesis pathway in human and mouse kidneys. a, Simplified de novo NAD$^+$ synthesis pathway. The colour indicates metabolites significantly higher (red) or lower (blue) in injured kidneys of human and mice. **b**, Relative quantification of tryptophan, kynurenine, and quinolinate in human kidneys (Healthy control $n = 25$. KD $n = 25$). $^*P < 0.05$. NS, not significant. **c**, Relative quantification of tryptophan, kynurenine, and quinolinate in mouse kidneys (PBS $n = 4$. Cis $n = 4$). $^{**}P < 0.01$, $^{***}P < 0.001$. **d**, Heatmap showing the expression of genes involved in NAD$^+$ metabolism in human kidneys. Color indicates higher (red) or lower (blue) expression. **e**, Heatmap showing the expression of genes involved in NAD$^+$ metabolism in mouse kidneys. Color indicates higher (red) or lower (blue) expression. Data are presented as mean ± s.e.m. and were analysed using a two-tailed Student's *t*-test.

https://doi.org/10.1038/s42255-023-00761-7

A

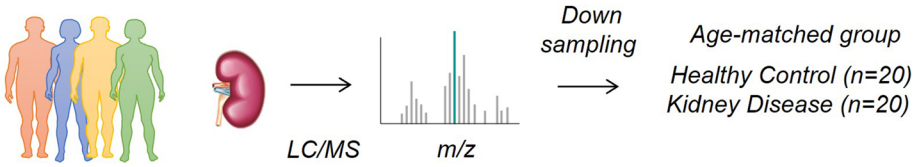

Clinical data	Healthy control	kidney disease	Significance
n	20	20	N.S.
eGFR ± SD	93 ± 16	31 ± 9.6	p < 0.001
Age ± SD	62 ± 7.6	64 ± 7.2	N.S.
Male (n)	13	13	N.S.
Female (n)	7	7	N.S.
Diabetes (n)	8	11	N.S.
Hypertension (n)	15	17	N.S.

B

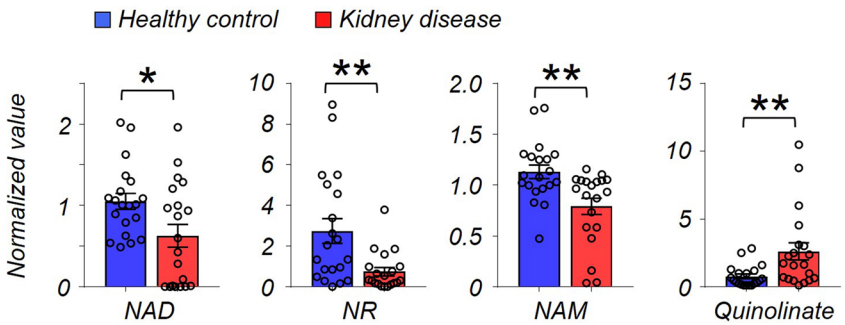

Extended Data Fig. 2 | Changes in de novo NAD$^+$ synthesis pathway in age-matched human kidneys. a, Demographic and clinical data of age-matched human kidney samples. **b**, Relative quantification of NAD$^+$, NR, NAM, and quinolinate in human kidneys (Healthy control $n = 25$. KD $n = 25$). *$P < 0.05$. Data are presented as mean ± s.e.m. and were analyzed using a two-tailed Student's t-test.

https://doi.org/10.1038/s42255-023-00761-7

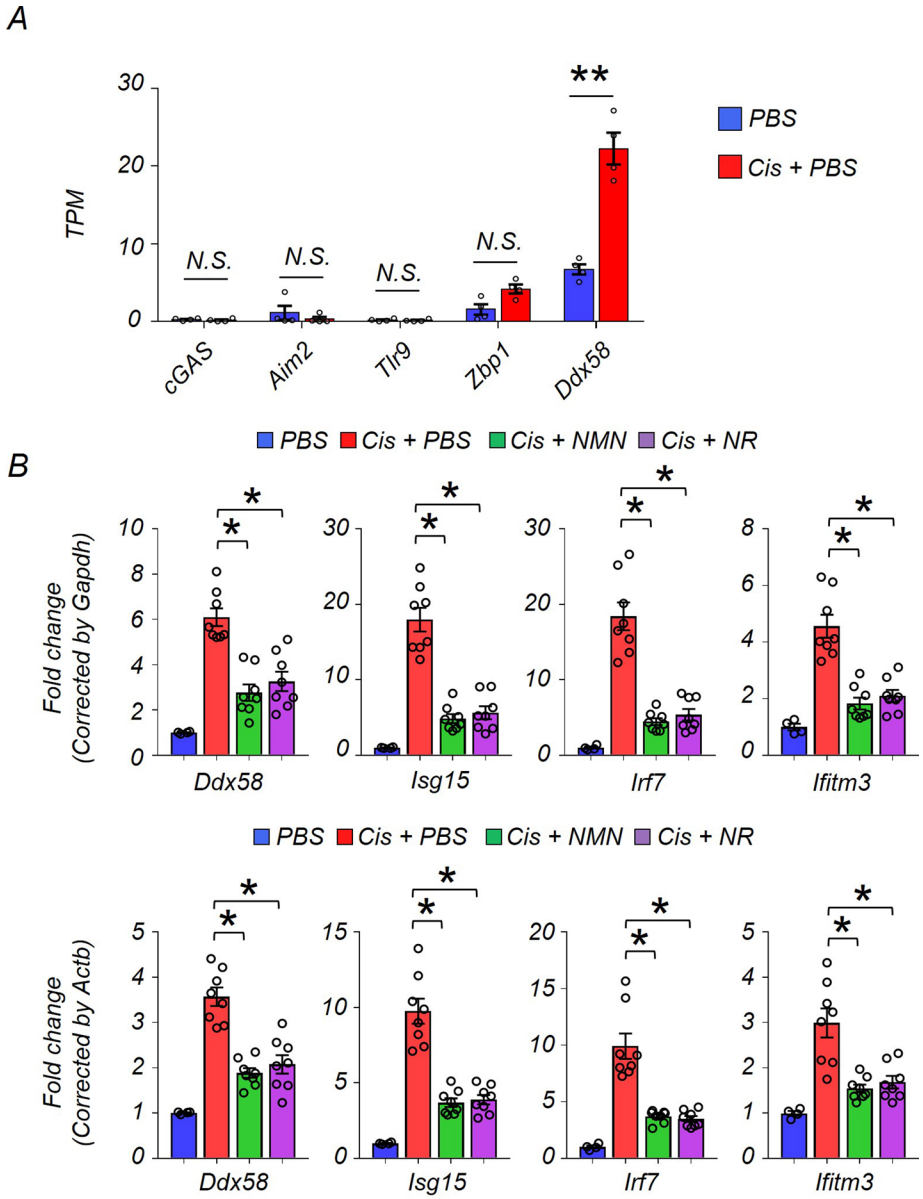

Extended Data Fig. 3 | The expression levels of genes involved in cytosolic DNA and RNA sensing in kidneys. a, TPM values of *cGAS, Aim2, Tlr9, Zbp1*, and *Ddx58* in kidneys. **b**, Relative transcript levels of *Ddx58, Isg15, Irf7*, and *Ifitm3* in in the kidneys of experimental groups (PBS $n = 4$. Cis + PBS $n = 8$. Cis + NMN $n = 8$. Cis + NR $n = 8$). Upper: Data were normalized using *Gapdh*. Lower; Data were normalized using *Actb*. Data are presented as mean ± s.e.m. and were analyzed using a one-way ANOVA followed by Tukey post hoc test for multigroup comparison.

https://doi.org/10.1038/s42255-023-00761-7

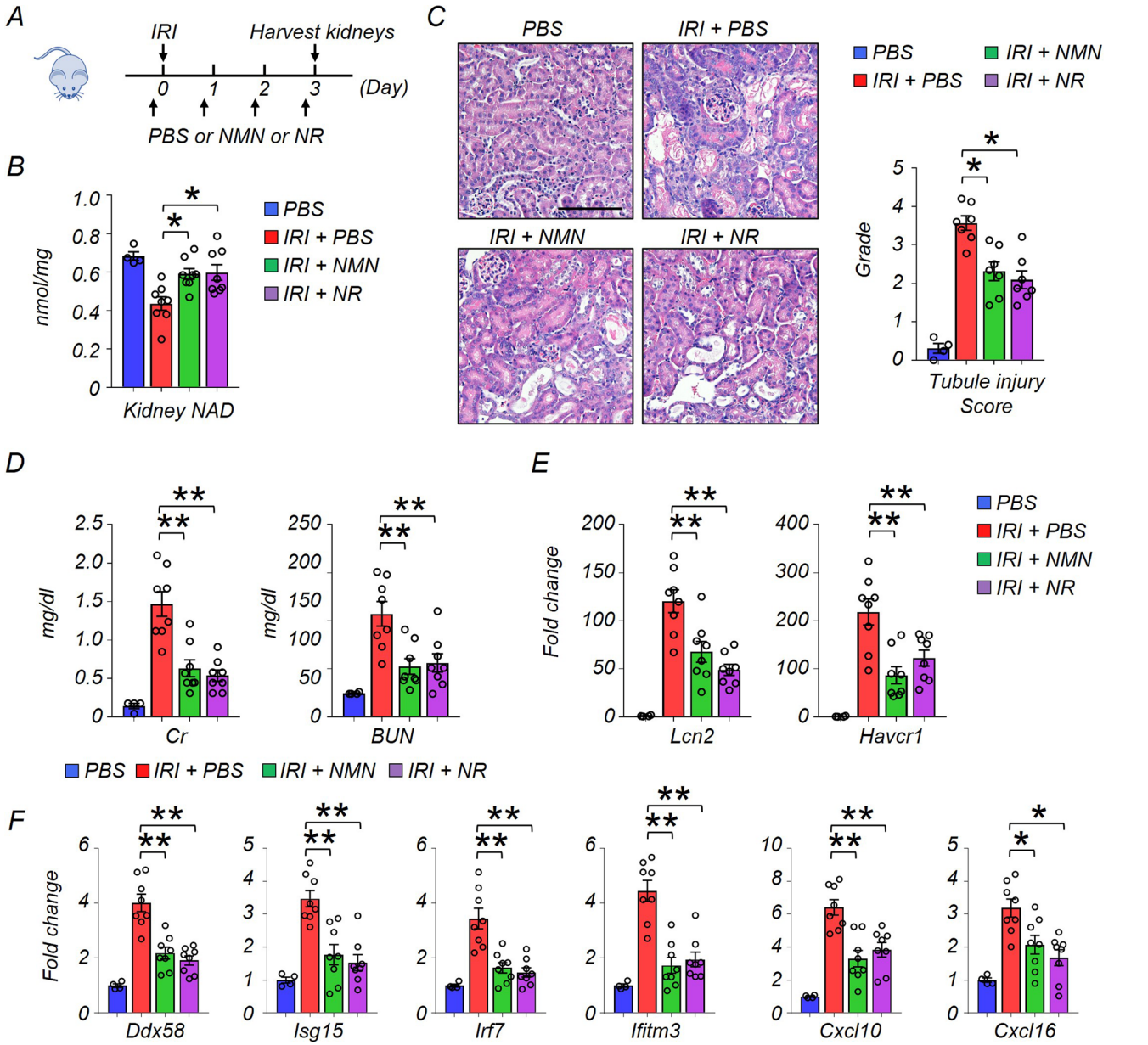

Extended Data Fig. 4 | NMN and NR supplementation improved kidney function and lowered inflammation in IRI mouse KD model. a, The experiment designs. NAD^+ precursors (NMN or NR) or vehicle (PBS) were injected i.p. for 4 consecutive days. First dose was injected 2 h before IRI. Kidneys were collected 3 days after IRI. **b**, Kidney NAD^+ levels in experimental groups. $^*P < 0.05$. **c**, Representative images of hematoxylin and eosin staining and semi-quantitative analysis of tubule injury in experimental groups. Scale bars: 20 μm. $^*P < 0.05$. **d**, Serum creatinine and blood urea nitrogen (BUN) levels in experimental groups. $^{**}P < 0.01$. **e**, Relative expression levels of *Lcn2* and *Havcr1* in the kidneys of mice in experimental groups. $^{**}P < 0.01$. **f**, Relative expression levels of *Ddx58, Isg15, Irf7, ifitm3, Cxcl10*, and *Cxcl16* in the kidneys of mice in experimental groups. $^*P < 0.05$, $^{**}P < 0.01$. **b**-**f**, PBS $n = 4$. Cis + PBS $n = 8$. Cis + NMN $n = 8$. Cis + NR $n = 8$. Data are presented as mean ± s.e.m. and were analyzed using a one-way ANOVA followed by Tukey post hoc test for multigroup comparison.

https://doi.org/10.1038/s42255-023-00761-7

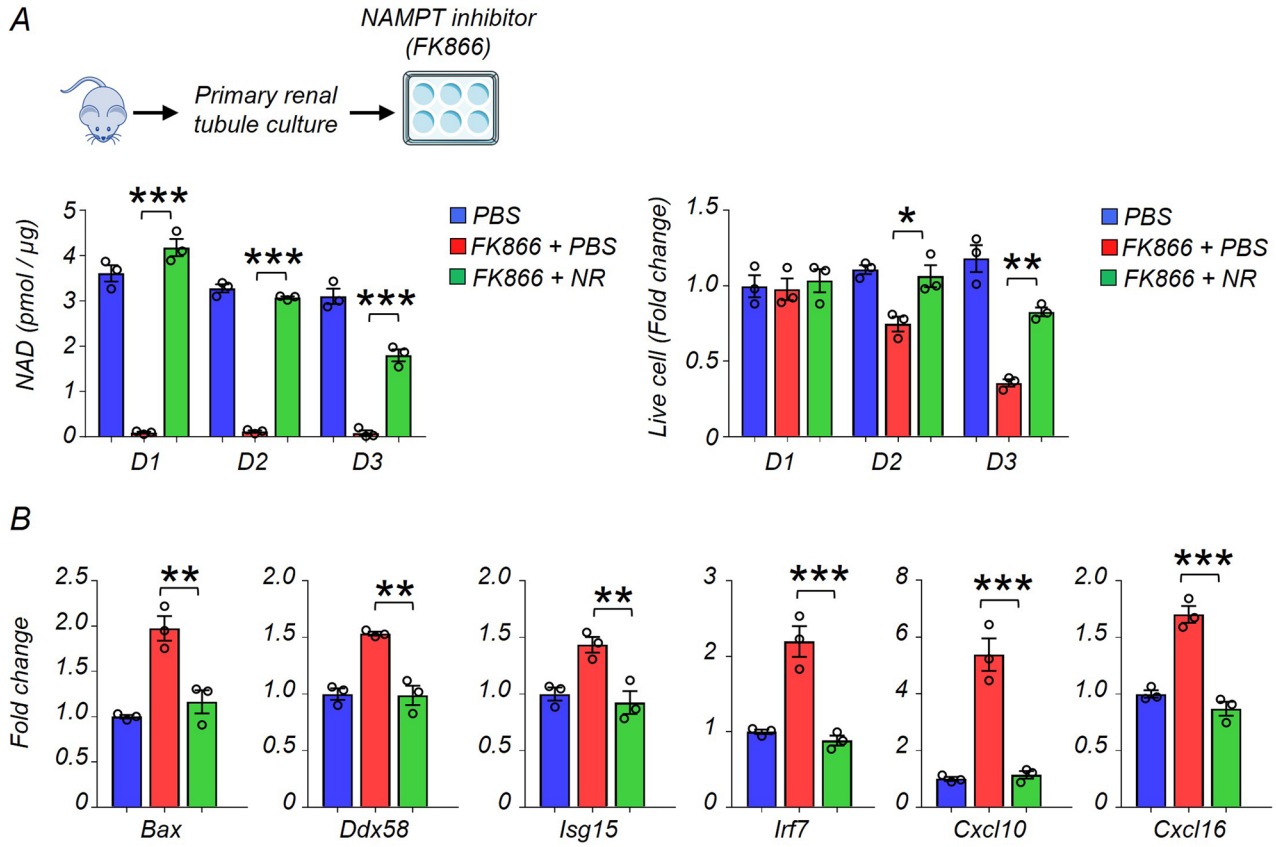

Extended Data Fig. 5 | The effect of NAD$^+$ depletion by NAMPT inhibitor (FK866). a, Experimental design. Renal tubule cells were cultured and treated with NAMPT inhibitor, FK866 (100 nM) for indicated days. NAD$^+$ levels in renal tubule cells and changes in live cell numbers of experimental groups on day1 (D1), day2 (D2), and day3 (D3). **b**, Relative transcript levels of *Bax, Ddx58, Isg15, Irf7, ifitm3, Cxcl10*, and *Cxcl16* in renal tubule cells of experimental groups on D2. Gene expression levels were normalized to *Gapdh*. (A, B) PBS $n = 3$. FK866 + PBS $n = 3$. FK866 + NR $n = 3$. Data are presented as mean ± s.e.m. and were analyzed using a one-way ANOVA followed by Tukey post hoc test for multigroup comparison.

https://doi.org/10.1038/s42255-023-00761-7

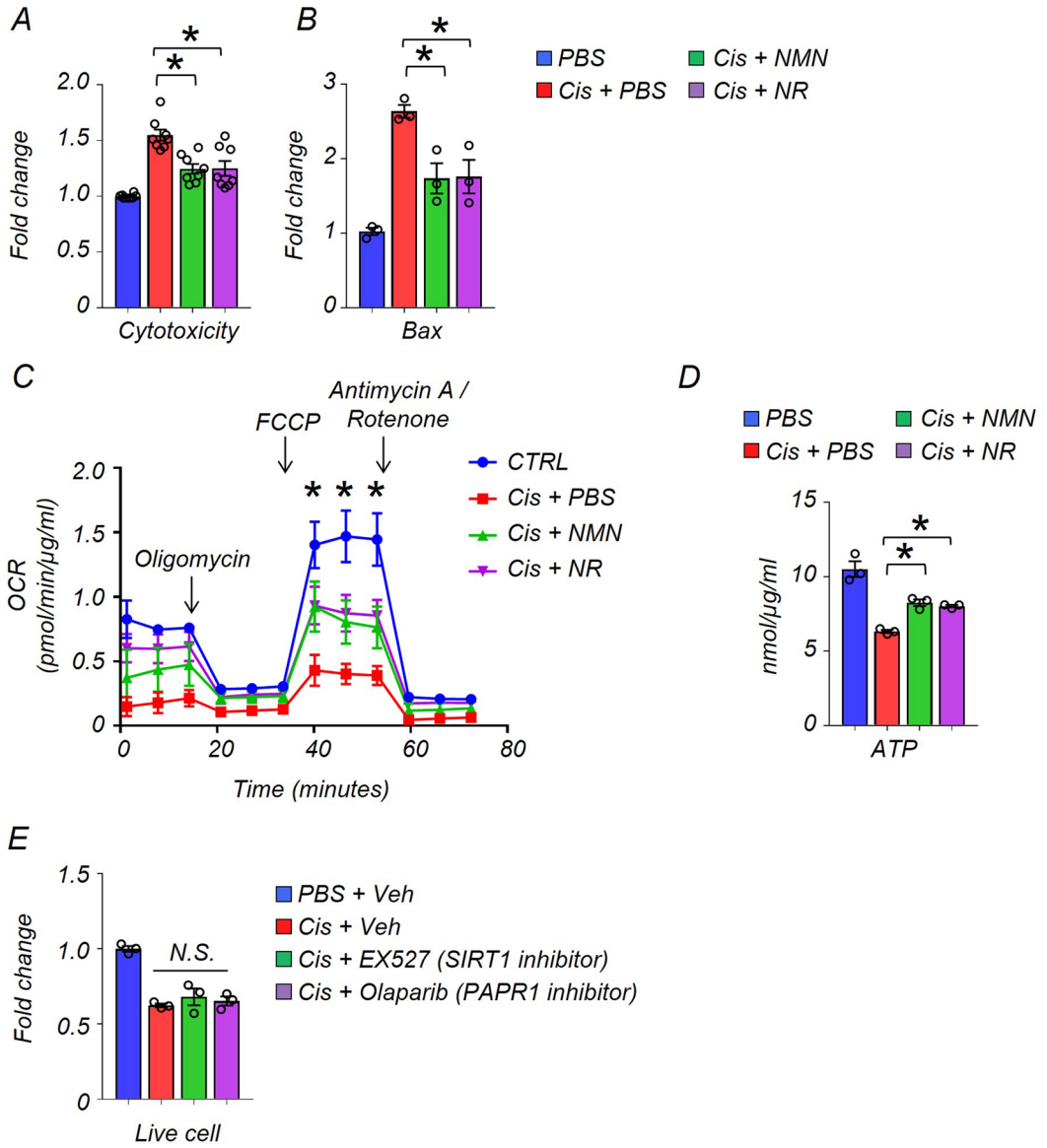

Extended Data Fig. 6 | NAD$^+$ precursors (NMN or NR) treatment restored mitochondria respiration capacity, lowered apoptosis, and improved energy production. a, Cytotoxicity assay. The data is as represented as fold change (FC) normalized to control PBS group ($n = 8$ in each group). **b**, Relative transcript levels of *Bax* in renal tubule cells of experimental groups ($n = 3$ in each group). Gene expression levels were normalized to *Gapdh*. **c**, The result of oxygen consumption rate (OCR) in cultured renal tubule cells of experimental groups PBS $n = 6$. Cis + PBS $n = 6$. Cis + NMN $n = 5$. Cis + NR $n = 5$. *$P < 0.05$. The data was normalized to total protein levels. **d**, ATP levels in renal tubule cells in experimental groups ($n = 3$ in each group). *$P < 0.05$. The data was normalized to total protein levels. **e**, Live cell numbers of cisplatin-treated renal tubule cells in indicated experiment groups ($n = 3$ in each group). veh; vehicle control. NS, not significant. Data are presented as mean ± s.e.m. and were analyzed using a one-way ANOVA followed by Tukey post hoc test for multigroup comparison.

https://doi.org/10.1038/s42255-023-00761-7

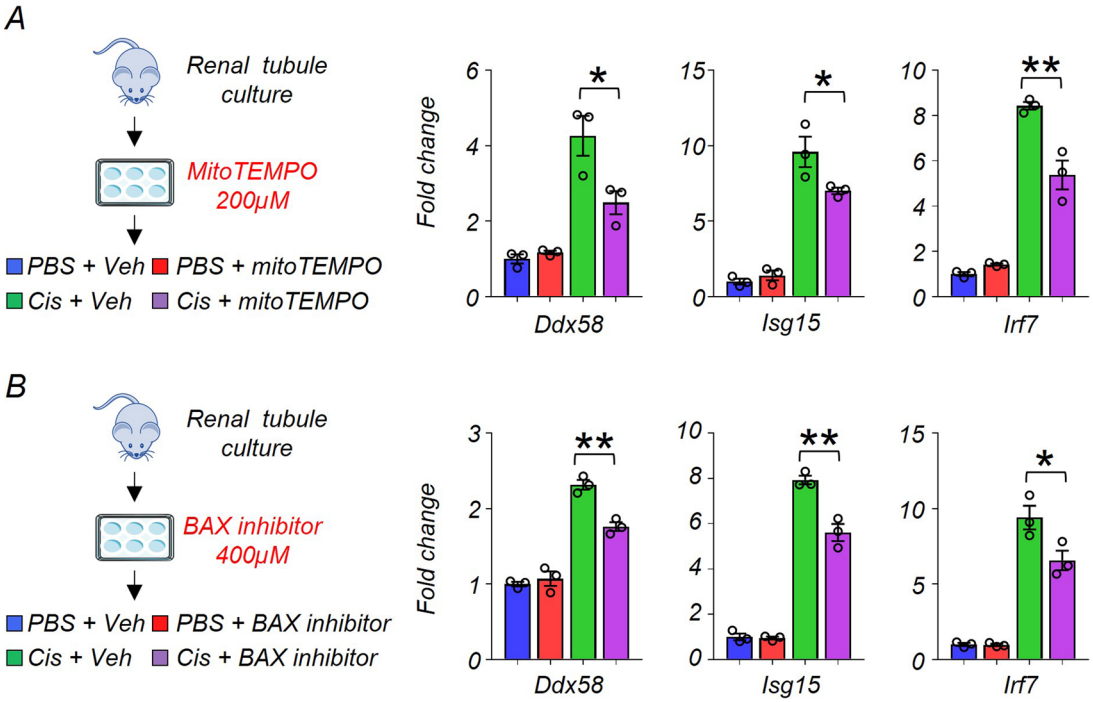

Extended Data Fig. 7 | MitoTEMPO and BAX inhibitor reduced RIG-I cytosolic RNA sensing pathway induction in renal tubule cells. a, (Left) The experimental design of the MitoTEMPO study. (Right) Relative transcript levels of *Ddx58, isg15*, and *Irf7* in experimental groups ($n = 3$ in each group). Gene expression levels were normalized using Gapdh. veh; vehicle control. *$P < 0.05$. **b**, (Left) The experimental design of the BAX inhibitor study. (Right) Relative transcript levels of *Ddx58, isg15*, and *Irf7* in experimental groups ($n = 3$ in each group). Gene expression levels were normalized using Gapdh. veh; vehicle control. *$P < 0.05$. Data are presented as mean ± s.e.m. and were analyzed using a one-way ANOVA followed by Tukey post hoc test for multigroup comparison.

https://doi.org/10.1038/s42255-023-00761-7

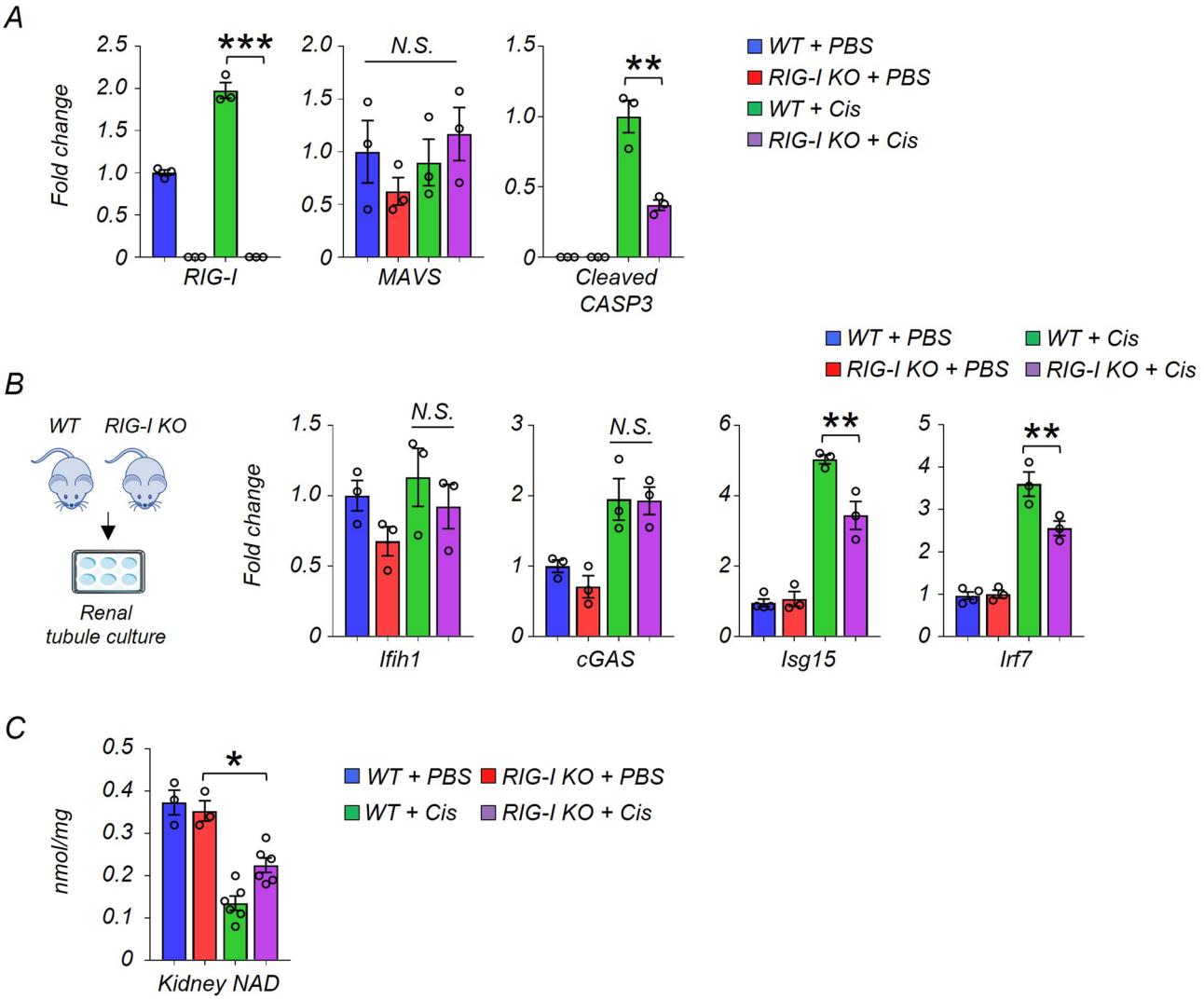

Extended Data Fig. 8 | RIG-I depletion protected from kidney injury, cell death, and inflammation. a, Western blot quantification of RIG-I, MAVS, cleaved caspase-3 (cCASP3) in mice kidneys in indicated groups ($n = 3$ in each group). $^*P < 0.05$, $^{***}P < 0.001$. NS, not significant. **b**, Experimental design. Renal tubule cells were isolated from WT and RIG-I KO mice. Relative transcript levels of *Ifih1, cGAS*, *Isg15* and *Irf7* in renal tubule cells of experimental groups ($n = 3$ in each group). Gene expression levels were normalized to *Gapdh*. $^*P < 0.05$. NS, not significant. **c**, Kidney NAD^+ levels in experimental groups (WT + PBS $n = 4$. RIG-I KO + PBS $n = 4$. WT + Cis $n = 6$. RIG-I KO + Cis $n = 6$). $^*P < 0.05$. Data are presented as mean ± s.e.m. and were analyzed using a one-way ANOVA followed by Tukey post hoc test for multigroup comparison.

https://doi.org/10.1038/s42255-023-00761-7

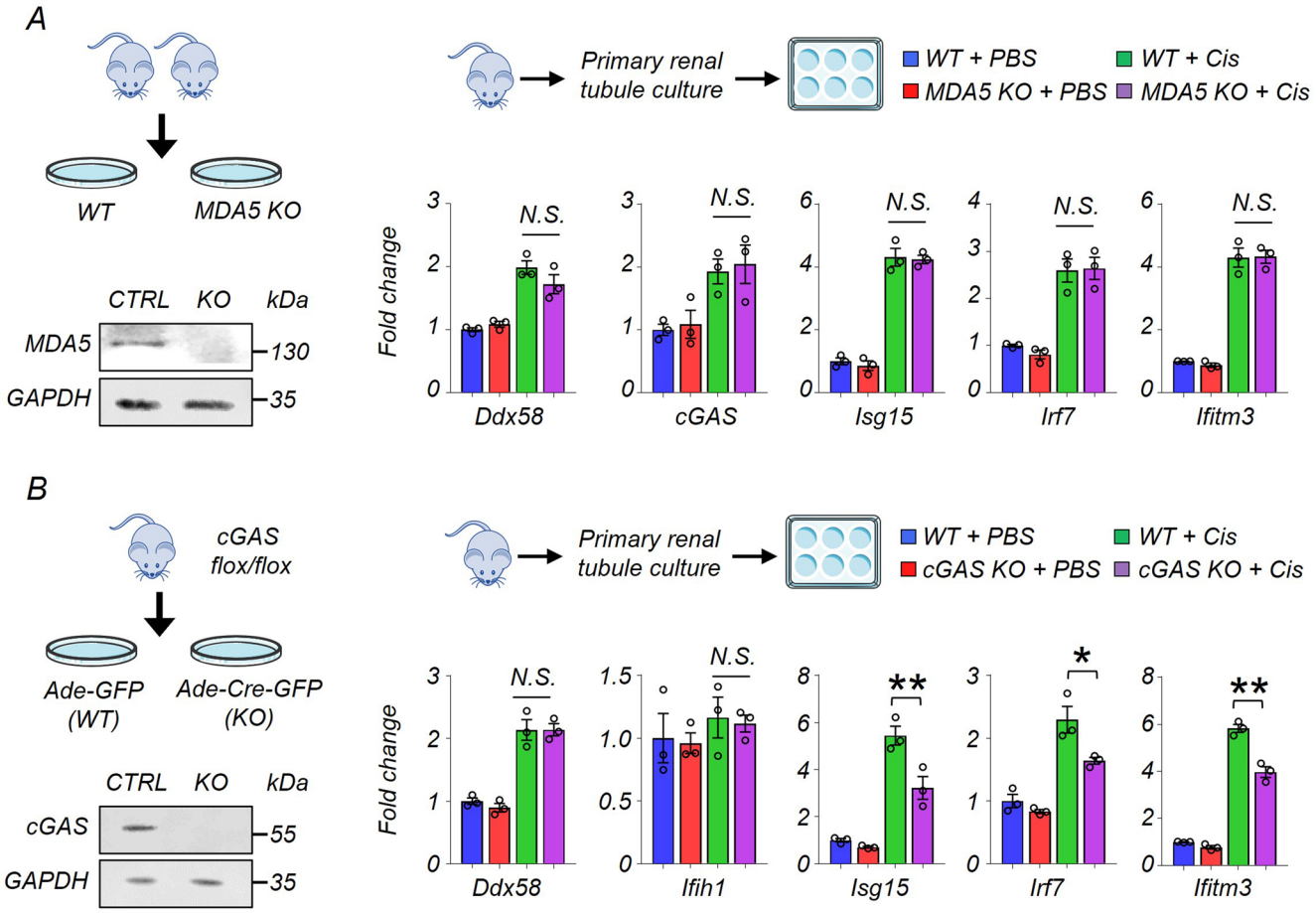

Extended Data Fig. 9 | The effect of MDA5 and cGAS deletion on expression of inflammatory molecules in cisplatin treated renal tubule cells. **a**, Experimental design. Renal tubule cells were isolated from WT and MDA5 KO mice. Western blot image of MDA5 in renal tubule cells. Relative transcript levels of *Ddx58*, *cGAS*, *Isg15*, *Irf7*, and *Ifitm3* in experimental groups ($n = 3$ in each group). Gene expression levels were normalized to *Gapdh*. NS, not significant. **b**, Experimental design. Renal tubule cells were isolated from cGAS flox/flox mice, and infected with Adenovirus-GFP (Ade-GFP) or Adenovirus-Cre-GFP (Ade-Cre-GFP). Western blot image of cGAS in renal tubule cells. Relative transcript levels of *Ddx58, Ifih1, Isg15, Irf7*, and *Ifitm3* in experimental groups ($n = 3$ in each group). Gene expression levels were normalized to *Gapdh*. $^*P < 0.05$. NS, not significant. Data are presented as mean ± s.e.m. and were analyzed using a one-way ANOVA followed by Tukey post hoc test for multigroup comparison.

https://doi.org/10.1038/s42255-023-00761-7

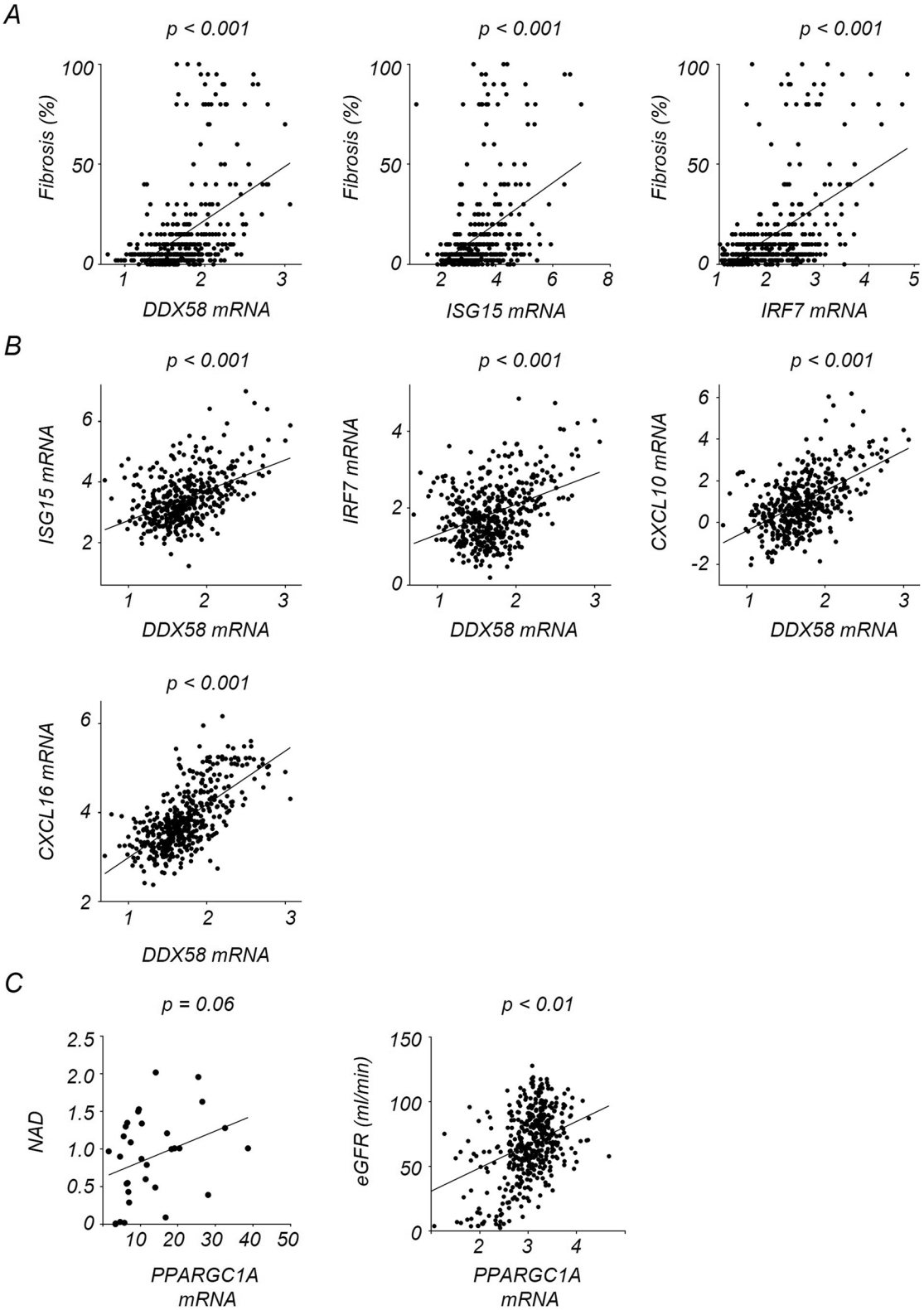

Extended Data Fig. 10 | The correlation between the degree of renal fibrosis and expression of RIG-I and cytosolic RNA sensing pathway genes. **a**, Correlation between the degree of kidney fibrosis and normalized transcription levels of *DDX58*, *ISG15*, and *IRF7* in human kidney samples. **b**, Correlation between transcription levels of *DDX58* and *ISG15*, *IRF7*, *CXCL10*, and *CXCL16* in human kidney samples. **c**, Correlation of relative transcript levels of *PPARGC1A* with kidney NAD^+ levels and eGFR. *P* value was calculated by Pearson's correlation.

nature portfolio

Corresponding author(s): Katalin Susztak

Last updated by author(s): Feb 4, 2023

Reporting Summary

Nature Portfolio wishes to improve the reproducibility of the work that we publish. This form provides structure for consistency and transparency in reporting. For further information on Nature Portfolio policies, see our Editorial Policies and the Editorial Policy Checklist.

Statistics

For all statistical analyses, confirm that the following items are present in the figure legend, table legend, main text, or Methods section.

n/a	Confirmed	
☐	☒	The exact sample size (*n*) for each experimental group/condition, given as a discrete number and unit of measurement
☐	☒	A statement on whether measurements were taken from distinct samples or whether the same sample was measured repeatedly
☐	☒	The statistical test(s) used AND whether they are one- or two-sided *Only common tests should be described solely by name; describe more complex techniques in the Methods section.*
☐	☒	A description of all covariates tested
☐	☒	A description of any assumptions or corrections, such as tests of normality and adjustment for multiple comparisons
☐	☒	A full description of the statistical parameters including central tendency (e.g. means) or other basic estimates (e.g. regression coefficient) AND variation (e.g. standard deviation) or associated estimates of uncertainty (e.g. confidence intervals)
☐	☒	For null hypothesis testing, the test statistic (e.g. *F*, *t*, *r*) with confidence intervals, effect sizes, degrees of freedom and *P* value noted *Give P values as exact values whenever suitable.*
☒	☐	For Bayesian analysis, information on the choice of priors and Markov chain Monte Carlo settings
☒	☐	For hierarchical and complex designs, identification of the appropriate level for tests and full reporting of outcomes
☐	☒	Estimates of effect sizes (e.g. Cohen's *d*, Pearson's *r*), indicating how they were calculated

Our web collection on statistics for biologists contains articles on many of the points above.

Software and code

Policy information about availability of computer code

Data collection	Kidneys from mice and human were collected and weighted for unbiased metabolomics study. Samples were prepared using the automated MicroLab STAR® system from Hamilton Company. For RNA-seq, total RNA was isolated from the kidneys of mice and human using the RNeasy mini kit (Qiagen #74126). Sequencing libraries were constructed using the Illumina TruSeq RNA Preparation Kit. High-throughput sequencing was performed using Illumina NovaSeq6000 with 100bp pair-end according to the manufacturer's instruction.
Data analysis	For metabolomics study, raw data was extracted, peak-identified and QC processed using Metabolon's hardware and software. These systems are built on a web-service platform utilizing Microsoft's NET technologies, which run on high-performance application servers and fiber-channel storage arrays in clusters to provide active failover and load-balancing. Compounds were identified by comparison to library entries of purified standards or recurrent unknown entities. For RNA-seq, adaptor and low-quality reads were trimmed using Trim-galore (version 0.6.5). Reads were aligned to the mouse (GRCm38) or human (hg19) reference genome using STAR (v2.4.1d). The aligned reads were mapped to the genes (GRCm38 or hg19) using HTSeq-0.6.1. Differentially expressed genes between experimental groups were identified using DESeq2 version 1.10.1. CIBERSORTx (version 1.0) was used to deconvolute (determine the percent of each cell type) the bulk RNA sequencing data of mouse kidney samples. The pathway analysis of metabolomics study was examined using MetaboAnalyst (version 5.0). Western blots were quantified using the Fiji software (version 2.1.0/1.53.c).

For manuscripts utilizing custom algorithms or software that are central to the research but not yet described in published literature, software must be made available to editors and reviewers. We strongly encourage code deposition in a community repository (e.g. GitHub). See the Nature Portfolio guidelines for submitting code & software for further information.

Data

Policy information about availability of data

All manuscripts must include a data availability statement. This statement should provide the following information, where applicable:

- Accession codes, unique identifiers, or web links for publicly available datasets
- A description of any restrictions on data availability
- For clinical datasets or third party data, please ensure that the statement adheres to our policy

Gene expression data presented in this paper are newly deposited to GSE207587. The RNA-seq data for large-scale human kidney samples are available in GSE115098. Mouse (GRCm38) or human (hg19) reference genome was used for gene mapping.

Human research participants

Policy information about studies involving human research participants and Sex and Gender in Research.

Reporting on sex and gender	We reported the number of male and female in the kidney metabolomics study. This was based on self-reported. The sample numbers of male and female are 30 and 20 respectively.
Population characteristics	We conducted metabolomics analysis for 50 human kidneys obtained from 25 healthy control or 25 patients with lower eGFR. The average of age is 58 and 68 respectively. Healthy control group includes 14 men, and 11 women, while patient group includes 16 men and 9 women. The detailed information is available in supplementary table 1 and 2.
Recruitment	De-identified human kidney samples were obtained via the Cooperative Human Tissue Network. Laboratory data including serum creatinine and demographic and clinical information was collected from medical records by an honest broker, therefore no informed consent was obtained from the subjects.
Ethics oversight	The University of Pennsylvania Institutional Review Board approved the study. The study was deemed IRB exempt (exemption IV).

Note that full information on the approval of the study protocol must also be provided in the manuscript.

Field-specific reporting

Please select the one below that is the best fit for your research. If you are not sure, read the appropriate sections before making your selection.

☒ Life sciences ☐ Behavioural & social sciences ☐ Ecological, evolutionary & environmental sciences

For a reference copy of the document with all sections, see nature.com/documents/nr-reporting-summary-flat.pdf

Life sciences study design

All studies must disclose on these points even when the disclosure is negative.

Sample size	No sample-size calculations for human and animal study were performed. Sample sizes were based on our experience and common practice in the related fields, balancing statistic robustness, resource availability. The paper by Doke et al., Single-cell analysis identifies the interaction of altered renal tubules with basophils orchestrating kidney fibrosis, Nature Immunology (2022) formed the basis of our sample size selection for in vivo experiments.
Data exclusions	No data was excluded.
Replication	Biological replicates are included to ensure the reproducibility and all repeated experiments are successful. For animal experiments, the number of replicates is equal to individual mice used. For in vivo study, at least six mice were used for each single groups and all experiments are independently repeated at least twice with similar results. For other experiments, at least two biological or technical replicates were included and performed independently to ensure the reproducibility. When representative data are shown, the experimental findings were reproduced independently with similar results.
Randomization	Randomisation was applied wherever possible. For animal experiments, age-matched mice are randomly assigned to different treatment and control groups. Otherwise, randomisation was not performed. For example, the mice kidney samples with highest RIN (RNA integrity number) were selected for RNA sequence library preparation. The same samples were analyzed in metabolomics study. When performing immunoblotting or immunostaining, samples were used in a specific order to generate the final figures. For human metabolomics study, 2 groups were assigned based on eGFR. However, each group was adjusted by the covariates including age , gender, hypertension, and diabetes.
Blinding	The samples were not blinded to the authors. All the experiments were objective and the conclusion were based on independent

Blinding	experiments, multiple technical replicates, and statistics significance. The information of the kidney function of human samples were known when we analyzed the data.

Reporting for specific materials, systems and methods

We require information from authors about some types of materials, experimental systems and methods used in many studies. Here, indicate whether each material, system or method listed is relevant to your study. If you are not sure if a list item applies to your research, read the appropriate section before selecting a response.

Materials & experimental systems

n/a	Involved in the study
☐	☒ Antibodies
☐	☒ Eukaryotic cell lines
☒	☐ Palaeontology and archaeology
☐	☒ Animals and other organisms
☒	☐ Clinical data
☒	☐ Dual use research of concern

Methods

n/a	Involved in the study
☒	☐ ChIP-seq
☒	☐ Flow cytometry
☒	☐ MRI-based neuroimaging

Antibodies

Antibodies used	Antibodies used for WB: RIG-I (D14G6) (CST, # 3743S,1:1000), cleaved Caspase-3 (CST, #9664,1:1000), BAX (CST, #2772,1:1000), MDA5 (CST #5321,1:1000), MAVS (CST, #4983S,1:1000), GAPDH (CST, #5174,1:1000), HSP60 (CST,#12165,1:1000), TIMM44(Sigma, #HPA043052, 1:1000), H3(CST,#9715,1:1000), cGAS (CST, #31659,1:1000). Horseradish peroxidase–conjugated secondary anti-rabbit or anti-mouse antibody (CST, #7074 and #7076, 1:5000) Antibodies used for immunofluorescence staining: FITC-labelled anti-mouse Ly-6G Antibody (BioLegend, #127605,1:500)
Validation	The following commercially available antibodies were validated by the company. RIG-I (D14G6) (CST, # 3743S), cleaved Caspase-3 (CST, #9664), BAX (CST, #2772), MDA5 (CST #5321), MAVS (CST, #4983S), GAPDH (CST, #5174), HSP60 (CST,#12165), TIMM44(Sigma, #HPA043052), H3(CST,#9715), cGAS (CST, #31659). Horseradish peroxidase–conjugated secondary anti-rabbit (CST, #7074) or anti-mouse antibody (CST,#7076). FITC-labelled anti-mouse Ly-6G Antibody (BioLegend, #127605)

Eukaryotic cell lines

Policy information about cell lines and Sex and Gender in Research

Cell line source(s)	Renal tubule cells were isolated from mice kidney and cultured. To delete mtDNA/RNA (Rho0 cells), cultured renal tubule cells were incubated iwith ethidium bromide (EtBr,100ng/ml) for 8 days.
Authentication	We used established protocol to culture renal tubule cells.
Mycoplasma contamination	The signature of mycoplasma contamination was not detected in all experiments.
Commonly misidentified lines (See ICLAC register)	No commonly misidentified cell lines were used in the study.

Animals and other research organisms

Policy information about studies involving animals; ARRIVE guidelines recommended for reporting animal research, and Sex and Gender in Research

Laboratory animals	All mouse experiments were performed between 8 to 12 weeks. We used C57BL/6 genetic background mice and mice were housed under Specific Pathogen Free (SPF) conditions with a 12 hour dark/light cycle, 22–25 °C, and 50-60% humidity with water and food provided ad libitum. RIG-I KO (Stock #046070), MAVS KO (Stock #008634), and MDA5 KO (Stock #015812) mice were obtained from Jackson Laboratory. cGAS flox mice were obtained from Charles Rice (Rockefeller University).
Wild animals	No wild animals were used.
Reporting on sex	Only Male mice were used in the study. The following experimental group were assigned. PBS; n=4, Cisplatin; n=8, Cisplatin with NMN; n=8, Cisplatin with NR; n=8.
Field-collected samples	The study did not involve samples collected from the field.
Ethics oversight	Animal studies were approved by the Institutional Animal Care and Use Committee (IACUC) of the University of Pennsylvania.

Note that full information on the approval of the study protocol must also be provided in the manuscript.